

An Effective Model of the Retinoic Acid Induced HL-60 Differentiation Program

Ryan Tasseff, Holly A. Jensen, Johanna Congleton[†], Wei Dai, Katherine Rogers, Adithya Sagar, Rodica P. Bunaciu[†], Andrew Yen[†], and Jeffrey D. Varner*

Robert Frederick Smith School of Chemical and Biomolecular Engineering and [†]Department of Biomedical Sciences, Cornell University, Ithaca NY 14853

Running Title: Effective modeling of HL-60 differentiation

To be submitted: ?

*Corresponding author:

Jeffrey D. Varner,

Professor, Robert Frederick Smith School of Chemical and Biomolecular Engineering,
244 Olin Hall, Cornell University, Ithaca NY, 14853

Email: jdv27@cornell.edu

Phone: (607) 255 - 4258

Fax: (607) 255 - 9166

Abstract

In this study, we present an effective model All-Trans Retinoic Acid (ATRA)-induced differentiation of HL-60 cells. The model describes a key architectural feature of ATRA-induced differentiation, positive feedback between an ATRA-inducible signalsome complex involving many proteins including Vav1, a guanine nucleotide exchange factor, and the activation of the mitogen activated protein kinase (MAPK) cascade. The model, which was developed by integrating logical rules with kinetic modeling, was significantly smaller than previous models. However, despite its simplicity, it captured key features of ATRA induced differentiation of HL-60 cells. We identified an ensemble of effective model parameters using measurements taken from ATRA-induced HL-60 cells. Using these parameters, model analysis predicted that MAPK activation was bistable as a function of ATRA exposure. Conformational experiments supported ATRA-induced bistability. These findings, combined with other literature evidence, suggest that positive feedback is central to a diversity of cell fate programs.

1 Introduction

2 Understanding the architecture of differentiation programs is an important therapeutic
3 challenge. Differentiation induction chemotherapy (DIC), using agents such as the vita-
4 min A derivative all-trans retinoic acid (ATRA), is a promising approach for the treatment
5 of many cancers (1–3). For example, ATRA treatment induces remission in 80–90% of
6 promyelocytic leukemia (APL) PML-RAR α -positive patients (4), thereby transforming a
7 fatal diagnosis into a manageable disease. However, remission is sometimes not durable
8 and relapsed cases exhibit emergent ATRA resistance (5, 6). To understand the basis of
9 this resistance, we must first understand the ATRA-induced differentiation program. To-
10 ward this challenge, lessons learned in model systems, such as the lineage-uncommitted
11 human myeloblastic cell line HL-60, could inform our analysis of the more complex dif-
12 ferentiation programs occurring in patients. Patient derived HL-60 leukemia cells have
13 been a durable experimental model since the 1970's to study differentiation (7). HL-60
14 undergoes cell cycle arrest and either myeloid or monocytic differentiation following stim-
15 ulation; ATRA induces G1/G0-arrest and myeloid differentiation in HL-60 cells, while 1,25-
16 dihydroxy vitamin D3 (D3) induces arrest and monocytic differentiation. Commitment to
17 cell cycle arrest and differentiation requires approximately 48 hr of treatment, during which
18 HL-60 cells undergo two division cycles.

19 Sustained mitogen-activated protein kinase (MAPK) activation is a defining feature of
20 ATRA-induced HL-60 differentiation. ATRA drives sustained MEK-dependent activation
21 of the Raf/MEK/ERK pathway, leading to arrest and differentiation (8). MEK inhibition re-
22 sults in the loss of ERK and Raf phosphorylation, and the failure to arrest and differentiate
23 (9). ATRA (and its metabolites) are ligands for the hormone activated nuclear transcrip-
24 tion factors retinoic acid receptor (RAR) and retinoid X receptor (RXR) (10). RAR/RXR
25 activation is necessary for ATRA-induced Raf phosphorylation (9), and the formation of
26 an ATRA-inducible signalsome complex at the membrane which drives MAPK activation

27 through a yet to be identified kinase activity. While the makeup of the signalsome com-
28 plex is not yet known, we do know that it is composed of Src family kinases Fgr and Lyn,
29 PI3K, c-Cbl, Slp76, and KSR, as well as IRF-1 transcription factors (11–15). Signalsome
30 formation and activity is driven by ATRA-induced expression of CD38 and the putative
31 heterotrimeric Gq protein-coupled receptor BLR1 (16, 17). BLR1, identified as an early
32 ATRA (or D3)-inducible gene using differential display (18), is necessary for MAPK ac-
33 tivation and differentiation (17), and is also involved with signalsome activity. Studies
34 of the BLR1 promoter identified a 5' 17bp GT box approximately 1 kb upstream of the
35 transcriptional start that conferred ATRA responsiveness (17). Members of the BLR1
36 transcriptional activator complex, e.g. NFATc3 and CREB, are phosphorylated by ERK,
37 JNK or p38 MAPK family members suggesting positive feedback between the signalsome
38 and MAPK activation (19). BLR1 overexpression enhanced Raf phosphorylation and ac-
39 celerated terminal differentiation, while Raf inhibition reduced BLR1 expression and dif-
40 ferentiation (20). BLR1 knock-out cells failed to activate Raf or differentiate in the pres-
41 ence of ATRA (20). Interestingly, both the knockdown or inhibition of Raf, also reduced
42 BLR1 expression and functional differentiation (20). Thus, the expression of signalsome
43 components e.g., BLR1 was Raf dependent, while Raf activation depended upon the sig-
44 nalsome. A previous computational study of ATRA-induced differentiation in HL-60 cells
45 suggested that the BLR1-MAPK positive feedback circuit was sufficient to explain ATRA-
46 induced sustained MAPK activation, and the expression of a limited number of functional
47 differentiation markers (21). Model analysis also suggested that Raf was the most distinct
48 of the MAPK proteins. However, this previous study developed and analyzed a complex
49 model, thus leaving open the critical question of what is the minimal positive feedback
50 circuit required to drive ATRA-induced differentiation.

51 In this study, we explored this question using a minimal mathematical model of the
52 key architectural feature of ATRA induced differentiation of HL-60 cells, namely positive

53 feedback between an ATRA-inducible signalsome complex and MAPK activation. The
54 ATRA responsive signalsome-MAPK circuit was then used to drive a downstream gene
55 expression program which encoded for the expression of intermediate and functional dif-
56 ferentiation markers. The effective model used a novel framework which integrated logi-
57 cal rules with kinetic modeling to describe gene expression and protein regulation, while
58 largely relying upon biophysical parameters from the literature. This formulation signifi-
59 cantly reduced the size and complexity of the model compared to the previous study of
60 Tasseff et al., while increasing the breadth of the biology described (21). The effective
61 model, despite its simplicity, captured key features of ATRA induced differentiation of HL-
62 60 cells. Model analysis predicted the bistability of MAPK activation as a function of ATRA
63 exposure; conformational experiments supported ATRA-induced bistability. Model simu-
64 lations were also consistent with measurements of the influence of MAPK inhibitors, and
65 the failure of BLR1 knockout cells to differentiate when exposed to ATRA. In addition, the
66 expression of intermediate and phenotypic differentiation markers as also captured follow-
67 ing ATRA exposure. Lastly, we showed by through immunoprecipitation studies, that the
68 guanine nucleotide exchange factor Vav1 is potentially a new ATRA-inducible member of
69 the signalsome complex. Taken together, these findings when combined with other litera-
70 ture evidence, suggested that positive feedback architectures are central to differentiation
71 programs generally, and necessary for ATRA-induced differentiation.

72 **Results**

73 We constructed an effective model of ATRA-induced HL-60 differentiation which described
74 signaling and gene expression events following the addition of ATRA (Fig. 1). The model
75 connectivity was developed from literature and the studies presented here (Table 1). We
76 decomposed the ATRA program into three modules; a signal initiation module that sensed
77 and transformed the ATRA signal into activated cRaf-pS621 and the ATRA-RXR/RAR
78 (Trigger) signals (Fig. 1A); a signal integration module that controlled the expression of
79 upstream transcription factors given cRaf-pS621 and activated Trigger signals (Fig. 1B);
80 and a phenotype module which encoded the expression of functional differentiation mark-
81 ers from the ATRA-inducible transcription factors (Fig. 1C). Each component of these
82 modules was described by a mRNA and protein balance equation. Additionally, the sig-
83 nal initiation module also described the abundance of activated species e.g., Trigger and
84 cRaf-pS621 whose values were derived from unactivated Trigger and cRaf protein levels.
85 Lastly, because the population of HL-60 cells was dividing (at least before ATRA-induced
86 cell cycle arrest), we also considered a dilution term in all balance equations. The sig-
87 nal initiation module contained nine differential equations, while the signal integration and
88 phenotype modules were collectively encoded by 54 differential equations. Model param-
89 eters were taken literature (Table 2), or estimated from experimental data using heuristic
90 optimization (see materials and methods).

91 The signal initiation module recapitulated sustained signalsome and MAPK activation
92 following exposure to $1\mu\text{M}$ ATRA (Fig. 2A-B). An ensemble of effective model param-
93 eters was estimated by minimizing the difference between simulations and time-series
94 measurements of BLR1 mRNA and cRaf-pS621 following the addition of $1\mu\text{M}$ ATRA. We
95 focused on the S621 phosphorylation site of cRaf since enhanced phosphorylation at
96 this site is a defining characteristic of sustained MAPK activation in HL-60. The effective
97 model captured both ATRA-induced BLR1 expression (Fig. 2A) and sustained phospho-

98 phosphorylation of cRaf-pS621 (Fig. 2B) in a growing population of HL-60 cells. Together, the
99 reinforcing positive feedback between the signalsome and MAPK led to sustained activation
100 over multiple cellular generations. However, the effective model failed to capture the
101 decline of BLR1 message after 48 hr of ATRA exposure. This suggested that we captured
102 the logic leading to the onset of differentiation, but failed to describe program shutdown.
103 Much of the focus in the literature has been on understanding the initiation of differenti-
104 ation, with little attention paid to understanding how a program is terminated. This is a
105 potential new direction that could be explored. Next, we tested the response of the signal
106 initiation module to different ATRA dosages.

107 The signal initiation model was bistable with respect to ATRA induction (Fig. 2C-D).
108 Phaseplane analysis predicted two stable steady-states when ATRA was present below
109 a critical threshold, and only a single steady-state above the threshold (Fig. 2C). In the
110 lower stable state, neither the signalsome nor cRaf-pS621 were present (thus, the differ-
111 entiation program was deactivated). However, at the high stable state, both the signal-
112 some and cRaf-pS621 were present, allowing for sustained activation and differentiation.
113 Interestingly, when ATRA was above a critical threshold, only the activated state was ac-
114 cessible (Fig. 2D). To test these findings, we first identified the ATRA threshold. We
115 exposed HL-60 cells to different ATRA concentrations for 72 hr (Fig. 2E). Morphological
116 changes associated with differentiation were visible for $\text{ATRA} \geq 0.25 \mu\text{M}$, suggesting the
117 critical ATRA threshold was near this concentration. Next, we conducted ATRA washout
118 experiments to determine if activated cells remained activated in the absence of ATRA.
119 HL-60 cells locked into an activated state remained activated following ATRA withdraw-
120 (Fig. 3). This sustained activation resulted from reinforcing feedback between the sig-
121 nalsome and the MAPK pathway. Thus, following activation, if we inhibited or removed
122 elements from the signal initiation module we expected the signalsome and MAPK signals
123 to decay. We simulated ATRA induced activation in the presence of kinase inhibitors, and

124 without key circuit elements. Consistent with experimental results using multiple MAPK
125 inhibitors, ATRA activation in the presence of MAPK inhibitors lowered the steady-state
126 value of signalsome (Fig. 3A). In the presence of BLR1, the signalsome and cRaf-pS621
127 signals were maintained following ATRA withdraw (Fig. 3B, gray). On the other hand,
128 BLR1 deletion removed the ability of the circuit to maintain a sustained MAPK response
129 following the withdraw of ATRA (Fig. 3B, blue). Lastly, washout experiments in which
130 cells were exposed to $1\mu\text{M}$ ATRA for 24 hr, and then transferred to fresh media with-
131 out ATRA, confirmed the persistence of the self sustaining activated state for up to 144
132 hr (Fig. 3C). Thus, these experiments confirmed that reinforcing positive feedback likely
133 drives the ATRA-induced differentiation program. Next, we analyzed the ATRA-induced
134 downstream gene expression program following signalsome and cRaf activation.

135 The signal integration and phenotype modules described ATRA-induced gene expres-
136 sion in wild-type HL-60 cells (Fig. 4). The signal initiation module produced two outputs,
137 activated Trigger and cRaf-pS621 which drove the expression of ATRA-induced transcrip-
138 tion factors, which then in turn activated the phenotypic program. In particular, Trigger (a
139 surrogate for the RAR α /RXR transcriptional complex) regulated the expression of the tran-
140 scription factors CCATT/enhancer binding protein α (C/EBP α), PU.1, and Egr-1. In turn,
141 these transcription factors, in combination with cRaf-pS621, regulated the expression of
142 downstream phenotypic markers such as CD38, CD11b or p47Phox. We assembled the
143 connectivity of the signal integration and phenotypic programs driven by Trigger and cRaf-
144 pS621 from literature (Table 1). We estimated the parameters for the signal initiation, and
145 phenotype modules from steady-state and dynamic measurements of transcription factor
146 and phenotypic marker expression following the addition of ATRA (22–25). However, the
147 bulk of the model parameters were taken from directly from literature (26) and were not
148 estimated in this study (see materials and methods). The model simulations captured the
149 time dependent expression of CD38 and CD11b following the addition ATRA (Fig. 4A),

150 and the steady-state for signal integration and phenotypic markers (Fig. 4B). Lastly, we
151 used the *predicted* values of the p21 and E2F protein abundance to estimate a black-
152 box model of ATRA-induced G0 arrest (Fig. 5). The phenotype module predicted p21
153 expression significantly increased and E2F expression decreased, in response to ATRA
154 exposure (Fig. 5A). We then used the ratio of these values in a polynomial model to cal-
155 culate the fraction of HL-60 cells in G0 arrest following the addition of ATRA (Fig. 5B). The
156 third-order polynomial model captured the trend in measured G0-arrest values as a func-
157 tion of time, and was robust to uncertainty in the measured data (Fig. 5B, gray). Taken
158 together, the output of the signal integration and phenotypic modules was consistent with
159 time-series and steady-state measurements, thereby validating the assumed molecular
160 connectivity. Moreover, outputs from the phenotype module described the trend in ATRA-
161 induced G0 cell cycle arrest. Next, we explored which nodes and interactions between
162 nodes in the signal integration module most influenced the system response.

163 The Gfi-1 and PPAR γ proteins were important regulators of ATRA-induced signal in-
164 tegration and phenotypic change (Fig. 6). We conducted pairwise gene knockout simula-
165 tions in the signal integration and phenotype modules to estimate which nodes controlled
166 the processing of the Trigger and cRaF-S621 signals. The difference between the sys-
167 tem state with and without the gene knockouts (encoded as a normalized state displace-
168 ment matrix) was decomposed using Singular Value Decomposition (SVD). A panel of
169 ten parameter sets was sampled, and the average normalized displacement matrix was
170 decomposed. The first six modes (approximately 36% of the total) described >95% of
171 the gene knockout variance, with the most important components of these modes being
172 the Gfi-1 and PPAR γ proteins, and to a lesser extent PU.1, C/EBP α and AP1 (Fig.
173 6A). To better understand which protein-DNA connections were important, we simulated
174 the pairwise deletion of interactions between these proteins and their respective regula-
175 tory targets. Singular value decomposition of the normalized state displacement matrix

assembled from the pairwise connection deletions, suggested the first six modes (approximately 26% of the total) accounted for >90% of the variance. Globally, the most sensitive interactions controlled p21 and p47Phox expression, markers for cell-cycle arrest and reactive oxygen formation phenotypic axes activated following ATRA addition (Fig. 6B). Analysis of the modes suggested the action of PPAR γ , Gfi-1 and C/EBP α were consistently important over multiple target genes. The connection knockout analysis also revealed robustness in the network. For example, no pair of deletions qualitatively changed the expression of regulators such as PU.1, Oct1, Oct4 or PPAR γ . Thus, the expression of these species was robust to disturbance in the connectivity. To better understand the combined influence of the PPAR γ and Gfi-1 deletions, we computed the fold change in the protein levels in the single (Gfi-1 $^{-/-}$ or PPAR γ $^{-/-}$) and double (Gfi-1 $^{-/-}$ and PPAR γ $^{-/-}$) mutants for the best fit parameter set (Fig. 7). Deletion of Gfi-1 led to a 2-4 fold increase in EGR-1, CD11b and C/EBP α expression, and a >8 fold increase in PU.1 abundance (Fig. 7,blue). On the other hand, deletion of PPAR γ led to >8 fold downregulation of CD38, p21, IRF1 and OCT1 (Fig. 7,red). Both knockouts slightly increased E2F expression, but neither influenced the expression of p47Phox. The double mutant was qualitatively similar to the combined behavior of the two single mutant cases. Taken together, Gfi-1 and PPAR γ controlled the cell-cycle arrest and receptor signaling axes, with PPAR γ regulating CD38, IRF1 and p21 expression while Gfi-1 controlled CD11b expression. These simulations suggested deletion of PPAR γ and Gfi-1 would not interfere with reactive oxygen formation, but would limit the ability of HL-60 cells to arrest. However, this analysis did not give insight into which components upstream of the signal initiation module were important. Toward this question, we explored the composition and regulation of the signalsome complex by experimentally interrogating a panel of possible Raf interaction partners.

The composition of the signalsome, and the kinase ultimately responsible for mediating ATRA-induced Raf activation is currently unknown. To explore this question, we

conducted immunoprecipitation and subsequent Western blotting to identify physical interactions between Raf and 19 putative interaction partners. A panel of 19 possible Raf interaction partners (kinases, GTPases, scaffolding proteins etc) was constructed based upon known signaling pathways. We did not consider the most likely binding partner, the small GTPase RAS, as previous studies have ruled it out in MAPK activation in HL-60 cells (20, 27). Total Raf was used as a bait protein for the immunoprecipitation studies. Interrogation of the Raf interactome suggested Vav1 was involved with ATRA-induced initiation of MAPK activity (Fig. 8). Western blot analysis using total Raf and pS621 Raf specific antibodies confirmed the presence of the bait protein, total and phosphorylated forms, in the immunoprecipitate (Fig. 8A). Of the 19 proteins sampled, Vav1, Src, CK2, Akt, and 14-3-3 precipitated with Raf, suggesting a direct physical interaction was possible. However, only the associations between Raf and Vav1, and Raf and Src were ATRA-inducible (Fig. 8). Furthermore, the Vav1 and Src associations were correlated with pS621 Raf abundance in the precipitate. Others proteins e.g., CK2, Akt and 14-3-3, generally bound Raf regardless of phosphorylation status or ATRA treatment. The remaining 14 proteins were expressed in whole cell lysate (Fig. 8B), but were not detectable in the precipitate of Raf IP. Treatment with the Raf kinase inhibitor GW5074 following ATRA exposure reduced the association of both Vav1 with Raf and Src with Raf (Fig. 8), although the signal intensity for Src was notably weak. However, GW5074 did not influence the association of CK2 or 14-3-3 with Raf, further demonstrating their independence from Raf phosphorylation. Interestingly, the Raf-Akt interaction qualitatively increased following treatment with GW5074; however, it remained unaffected by treatment with ATRA. Src family kinases are known to be important in myeloid differentiation (28) and their role in HL-60 differentiation has been investigated elsewhere (11). Given the existing work and variable reproducibility in the context of the Raf immunoprecipitate, we did not investigate the role of Src further in this study. Taken together, the immunoprecipitation and GW5074 results

228 implicated Vav1 association to be correlated with Raf activation following ATRA-treatment.
229 Previous studies demonstrated that a Vav1-Slp76-Cbl-CD38 complex plays an important
230 role in ATRA-induced MAPK activation and differentiation of HL-60 cells (13). Here we
231 did not observe direct interaction of Raf with Cbl or Slp76; however, this complex could
232 be involved upstream. Next, we considered the effect of the Raf kinase inhibitor GW5074
233 on functional markers of ATRA-induced growth arrest and differentiation.

234 Inhibition of Raf kinase activity modulated MAPK activation and differentiation mark-
235 ers following ATRA exposure (Fig. 8D-F). ATRA treatment alone statistically significantly
236 increased the G1/G0 percentage over the untreated control, while GW5074 alone had a
237 negligible effect on the cell cycle distribution (Fig. 8D). Surprisingly, the combination of
238 GW5074 and ATRA statistically significantly increased the G1/G0 population ($82 \pm 1\%$)
239 compared with ATRA alone ($61 \pm 0.5\%$). Increased G1/G0 arrest following the combined
240 treatment with GW5074 and ATRA was unexpected, as the combination of ATRA and the
241 MEK inhibitor (PD98059) has been shown previously to decrease ATRA-induced growth
242 arrest (8). However, growth arrest is not the sole indication of functional differentiation.
243 Expression of the cell surface marker CD11b has also been shown to coincide with HL-60
244 cells myeloid differentiation (29). We measured CD11b expression, for the various treat-
245 ment groups, using immuno-fluorescence flow cytometry 48 hr post-treatment. As with
246 G1/G0 arrest, ATRA alone increased CD11b expression over the untreated control, while
247 GW5074 further enhanced ATRA-induced CD11b expression (Fig. 8E). GW5074 alone
248 had no statistically significant effect on CD11b expression, compared with the untreated
249 control. Lastly, the inducible reactive oxygen species (ROS) response was used as a func-
250 tional marker of differentiated neutrophils (16). We measured the ROS response induced
251 by the phorbol ester 12-O-tetradecanoylphorbol-13-acetate (TPA) using flow cytometry.
252 Untreated cells showed no discernible TPA response, with only $7.0 \pm 3.0\%$ ROS induction
253 (Fig. 8F). Cells treated with ATRA had a significantly increased TPA response, $53 \pm 7\%$

254 ROS induction 48 hr post-treatment. Treatment with both ATRA and GW5074 statistically
255 significantly reduced ROS induction ($22 \pm 0.6\%$) compared to ATRA alone. Interestingly,
256 Western blot analysis did not detect a GW5074 effect on ATRA-induced expression of
257 p47Phox, a required upstream component of the ROS response (Fig. 8F, bottom). Thus,
258 the inhibitory effect of GW5074 on inducible ROS might occur downstream of p47Phox
259 expression. However, the ROS producing complex is MAPK dependent, therefore it is
260 also possible that GW5074 inhibited ROS production by interfering with MAPK activation
261 (in which case the p47Phox marker might not accurately reflect phenotypic conversion
262 and differentiation).

263 **Discussion**

264 In this study, we presented an effective model of ATRA-inducible differentiation of HL-60
265 cells. The model consisted of three modules: a signal initiation module that sensed and
266 transformed the ATRA signal into activated cRaf-pS621 and the ATRA-RXR/RAR (Trig-
267 ger) signals; a signal integration module that controlled the expression of upstream tran-
268 scription factors given cRaf-pS621 and activated Trigger signals; and a phenotype mod-
269 ule which encoded the expression of functional differentiation markers from the ATRA-
270 inducible transcription factors. The model described the transcription and translation of
271 genes in each module, and signaling events in each module in a growing population of
272 HL-60 cells. Model parameters were taken from literature, however, unknown coefficients
273 that appear in the promoter logic models were estimated from protein measurements in
274 HL-60 cells following ATRA exposure. Despite its simplicity, the effective model captured
275 key features of the ATRA induced differentiation such as sustained MAPK activation, and
276 bistability with respect to ATRA exposure. The model also described the expression of
277 upstream transcription factors which regulated the expression of differentiation markers.
278 Lastly, analysis of the response of the model to perturbations identified Gfi-1 and PPAR γ
279 as master regulators of ATRA-induced differentiation. We also reported a new ATRA-
280 inducible component of the signalsome, Vav1. Vav1 is a guanine nucleotide exchange
281 factor for Rho family GTPases that activate pathways leading to actin cytoskeletal re-
282 arrangements and transcriptional alterations (30). The Vav1/Raf association correlated
283 with Raf activity, was ATRA-inducible and decreased after treatment with the Raf inhibitor
284 GW5074.

285 Naturally occurring cell fate decisions often incorporate reinforcing feedback and bista-
286 bility (31, 32). One of the most well studied cell fate circuits is the Mos mitogen-activated
287 protein kinase cascade in *Xenopus* oocytes. This cascade is activated when oocytes are
288 induced by the steroid hormone progesterone (33). The MEK-dependent activation of p42

289 MAPK stimulates the accumulation of the Mos oncoprotein, which in turn activates MEK,
290 thereby closing the feedback loop. This is similar to the signal initiation module presented
291 here; ATRA drives signalsome formation, which activates MAPK, which in turn leads to
292 more signalsome activation. Thus, while HL-60 and *Xenopus* oocytes are vastly different
293 biological models, their cell fate programs share a similar architectural feature. Reinforc-
294 ing feedback and bistability has also been implicated in hematopoietic cell fate determi-
295 nation. Laslo et al showed in nonmalignant myelomonocytic cells that the counter antag-
296 onistic repressors, Gfi-1 and Egr-1/2 (whose expression is tuned by PU.1 and C/EBP α),
297 encode a bistable switch that results in a macrophage, neutrophil or a mixed lineage pop-
298 ulation depending upon PU.1 and C/EBP α expression (32). The current model contained
299 the Gfi-1 and Egr-1/2 agonistic switch; however, its significance was unclear for HL-60
300 cells. The expression of Gfi-1, Egr-1/2, C/EBP α and PU.1 was not consistent with the
301 canonical lineage pattern expected from literature. For example, Egr-1/2 expression (as-
302 sociated with a macrophage lineage) increased, while Gfi-1 expression (associated with
303 a neutrophil lineage) remained constant following ATRA exposure. Thus, HL-60 cells,
304 which are a less mature cancer cell line, exhibited a non-canonical expression pattern.
305 Other unrelated cell fate decisions such as programmed cell death have also been sug-
306 gested to be bistable (34). Still more biochemical networks important to human health,
307 for example the human coagulation or complement cascades, also feature strong positive
308 feedback elements (35). Thus, while reinforcing feedback is often undesirable in human
309 engineered systems, it is at the core of a diverse variety of cell fate programs and other
310 networks important to human health.

311 Analysis of the signal integration and phenotype modules suggested that Gfi-1 and
312 PPAR γ were required for ATRA-induced differentiation in HL-60 cells. Model analysis
313 showed that PU.1, Egr-1 and C/EBP α expression increased in Gfi-1 $^{-/-}$ mutants, where
314 PU.1 expression was upregulated by greater than 8-fold. PU.1, a member of the *ets* tran-

scription factor family, is a well known regulator of granulocyte and monocyte development (36). The relative level of PU.1 and C/EBP α is thought to control macrophage versus neutrophil cell fate decisions in granulocytic macrophage progenitor cells (37). Simulations suggested that combined Gfi-1 + PPAR γ deletion crippled the ability of HL-60 cells to undergo neutrophilic differentiation following ATRA exposure. p21 expression decreased significantly, suggesting Gfi-1 $^{-/-}$ + PPAR γ $^{-/-}$ mutants were less likely to G0-arrest following ATRA exposure. The expression of other neutrophilic markers, such as CD38, also decreased in Gfi-1 $^{-/-}$ + PPAR γ $^{-/-}$ cells. On the other hand, the expression of reactive oxygen metabolic markers, or other important transcription factors such as OCT4 did not change. For example, model analysis suggested that the C/EBP α dependent interaction of PU.1 with the *NCF1* gene, which encodes the p47Phox protein, was the most sensitive PU.1 connection; deletion of this connection removed the ability of the system to express p47Phox. p47Phox, also known as neutrophil cytosol factor 1, is one of four cytosolic subunits of the multi-protein NADPH oxidase complex found in neutrophils (38). This enzyme is responsible for reactive oxygen species (ROS) production, a key component of the anti-microbial function of neutrophils. While p47Phox expression required C/EBP α and PU.1, neither Gfi-1 nor PPAR γ deletion increased expression. This suggested that p47Phox expression was saturated with respect to C/EBP α and PU.1, and simultaneously not sensitive to PPAR γ abundance. Taken together, Gfi-1 $^{-/-}$ + PPAR γ $^{-/-}$ cells were predicted to exhibit some aspects of the ATRA response, but not other critical features such as cell cycle arrest. Hock et al showed that Gfi-1 $^{-/-}$ mice lacked normal neutrophils, and were highly sensitive to bacterial infection (39). Thus, the model analysis was consistent with this study. However, other predictions concerning the behavior of the Gfi-1 $^{-/-}$ + PPAR γ $^{-/-}$ mutants have yet to be verified experimentally.

Immunoprecipitation studies identified a limited number of ATRA-dependent and - independent Raf interaction partners. While we were unable to detect the association

341 of Raf with common kinases and GTPases such as PKC, PKA, p38, Rac and Rho, we
342 did establish potential interactions between Raf and key partners such as Vav1, Src, Akt,
343 CK2 and 14-3-3. All of these partners are known to be associated with Raf activation
344 or function. Src is known to bind Raf through an SH2 domain, and this association has
345 been shown to be dependent of the serine phosphorylation of Raf (40). Thus, an ATRA in-
346 ductible Src/Raf association may be a result of ATRA-induced Raf phosphorylation at S259
347 or S621. We also identified an interaction between Raf and the Ser/Thr kinases Akt and
348 CK2. Akt can phosphorylate Raf at S259, as demonstrated by studies in a human breast
349 cancer line (41). CK2 can also phosphorylate Raf, although the literature has traditionally
350 focused on S338 and not S621 or S259(42). However, neither of these kinase interactions
351 were ATRA-inducible, suggesting their association with Raf alone was not associated with
352 ATRA-induced Raf phosphorylation. The adapter protein 14-3-3 was also constitutively
353 associated with Raf. The interaction between Raf and 14-3-3 has been associated with
354 both S621 and S259 phosphorylation and activity (43). Additionally, the association of
355 Raf with 14-3-3 not only stabilized S621 phosphorylation, but also reversed the S621
356 phosphorylation from inhibitory to activating (44). Finally, we found that Vav1/Raf associ-
357 ation correlated with Raf activity, was ATRA-inducible and decreased after treatment with
358 GW5074. The presence of Vav1 in Raf/Grb2 complexes has been shown to correlate with
359 increased Raf activity in mast cells (45). Furthermore, studies on Vav1 knockout mice
360 demonstrated that the loss of Vav1 resulted in deficiencies of ERK signaling for both T-
361 cells as well as neutrophils (46, 47). Interestingly, while an integrin ligand-induced ROS
362 response was blocked in Vav1 knockout neutrophils, TPA was able to bypass the Vav1
363 requirement and stimulate both ERK phosphorylation and ROS induction (47). In this
364 study, the TPA-induced ROS response was dependent upon Raf kinase activity, and was
365 mitigated by the addition of GW5074. It is possible that Vav1 is downstream of various
366 integrin receptors but upstream of Raf in terms of inducible ROS responses. Vav1 has

367 also been shown to associate with a Cbl-Slp76-CD38 complex in an ATRA-dependent
368 manner; furthermore, transfection of HL-60 cells with Cbl mutants that fail to bind CD38,
369 yet still bind Slp76 and Vav1, prevents ATRA-induced MAPK activation (13). The literature
370 suggest a variety of possible receptor-signaling pathways, which involve Vav1, for MAPK
371 activation; moreover, given the ATRA-inducible association Vav1 may play a direct role in
372 Raf activation.

373 We hypothesized that Vav1 is a member of an ATRA-inducible complex which propels
374 sustained MAPK activation, arrest and differentiation. Initially, ATRA-induced Vav1 ex-
375 pression drives increased association between Vav1 and Raf. This increased interaction
376 facilitates phosphorylation and activation of Raf by pre-bound Akt and/or CK2 at S621
377 or perhaps S259. Constitutively bound 14-3-3 may also stabilize the S621 phosphory-
378 lation, modulate the activity and/or up-regulate autophosphorylation. Activated Raf can
379 then drive ERK activation, which in turn closes the positive feedback loop by activating
380 Raf transcription factors e.g., Sp1 and/or STAT1 (48–51). We tested this working hy-
381 pothesis using mathematical modeling. The model recapitulated both ATRA time-course
382 data as well as the GW5074 inhibitor effects. This suggested the proposed Raf-Vav1
383 architecture was at least consistent with the experimental studies. Further, analysis of
384 the Raf-Vav1 model identified bistability in ppERK levels. Thus, two possible MAPK ac-
385 tivation branches were possible for experimentally testable ATRA values. The analysis
386 also suggested the ATRA-induced Raf-Vav1 architecture could be locked into a sustained
387 signaling mode (high ppERK) even in the absence of a ATRA signal. This locked-in prop-
388 erty could give rise to an ATRA-induction memory. We validated the treatment memory
389 property predicted by the Raf-Vav1 circuit experimentally using ATRA-washout experi-
390 ments. ERK phosphorylation levels remained high for more then 96 hr after ATRA was
391 removed. Previous studies demonstrated that HL-60 cells possessed an inheritable mem-
392 ory of ATRA stimulus (52). Although the active state was self-sustaining, the inactive state

393 demonstrated considerable robustness to perturbation. For example, we found that 50x
394 overexpression of Raf was required to reliably lock MAPK into the activated state, while
395 small perturbations had almost no effect on ppERK levels over the entire ensemble. CD38
396 expression correlated with the ppERK, suggesting its involvement in the signaling com-
397 plex. Our computational and experimental results showed that positive feedback, through
398 ERK-dependent Raf expression, could sustain MAPK signaling through many division cy-
399 cles. Such molecular mechanisms could underly aspects of cellular memory associated
400 to consecutive ATRA treatments.

401 **Materials and Methods**

402 *Effective gene expression model equations.* We decomposed the ATRA-induced differ-
 403 entiation program into three modules; a signal initiation module that sensed and trans-
 404 formed the ATRA signal into activated cRaf-pS621 and the ATRA-RXR/RAR (activated
 405 Trigger) signals; a signal integration module that controlled the expression of upstream
 406 transcription factors given cRaf-pS621 and activated Trigger signals; and a phenotype
 407 module which encoded the expression of functional differentiation markers from the ATRA-
 408 inducible transcription factors. The output of the signal initiation module was the input to
 409 the gene expression model. For each gene $j = 1, 2, \dots, \mathcal{G}$, we modeled both the mRNA
 410 (m_j), protein (p_j) and signaling species abundance:

$$\frac{dm_j}{dt} = r_{T,j} - (\mu + \theta_{m,j}) m_j + \lambda_j \quad (1)$$

$$\frac{dp_j}{dt} = r_{X,j} - (\mu + \theta_{p,j}) p_j \quad (2)$$

$$g(p_1, \dots, p_{\mathcal{G}}, \kappa) = 0 \quad (3)$$

411 The terms $r_{T,j}$ and $r_{X,j}$ denote the specific rates of transcription, and translation while
 412 the terms $\theta_{m,j}$ and $\theta_{p,j}$ denote first-order degradation constants for mRNA and protein,
 413 respectively. The specific transcription rate $r_{T,j}$ was modeled as the product of a kinetic
 414 term $\bar{r}_{T,j}$ and a control term u_j which described how the abundance of transcription fac-
 415 tors, or other regulators influenced the expression of gene j . The kinetic transcription
 416 term $\bar{r}_{T,j}$ was modeled as:

$$\bar{r}_{T,j} = V_T^{max} \left(\frac{L_{T,o}}{L_{T,j}} \right) \left(\frac{G_j}{K_T + G_j} \right) \quad (4)$$

417 where the maximum gene expression rate V_T^{max} was defined as the product of a char-
 418 acteristic transcription rate constant (k_T) and the abundance of RNA polymerase (R_1),

419 $V_T^{max} = k_T(R_1)$. The $(L_{T,o}/L_{T,j})$ term denotes the ratio of transcription read lengths; $L_{T,o}$
 420 represents a characteristic gene length, while $L_{T,j}$ denotes the length of gene j . Thus, the
 421 ratio $(L_{T,o}/L_{T,j})$ is a gene specific correction to the characteristic transcription rate V_T^{max} .
 422 Lastly, the λ_j term denotes the constitutive rate of expression of gene j .

423 The gene expression control term $0 \leq u_j \leq 1$ depended upon the combination of fac-
 424 tors which influenced the expression of gene j . If the expression of gene j was influenced
 425 by $1, \dots, m$ factors, we modeled this relationship as $u_j = \mathcal{I}_j(f_{1j}(\cdot), \dots, f_{mj}(\cdot))$ where
 426 $0 \leq f_{ij}(\cdot) \leq 1$ denotes a regulatory transfer function quantifying the influence of factor i
 427 on the expression of gene j , and $\mathcal{I}_j(\cdot)$ denotes an integration rule which combines the
 428 individual regulatory inputs for gene j into a single control term. In this study, the integra-
 429 tion rule governing gene expression was the weighted fraction of promoter configurations
 430 that resulted in gene expression (53):

$$u_j = \frac{W_{R_{1,j}} + \sum_n W_{nj} f_{nj}}{1 + W_{R_{1,j}} + \sum_d W_{dj} f_{dj}} \quad (5)$$

431 The numerator, the weighted sum (with weights W_{nj}) of promoter configurations leading to
 432 gene expression, was normalized by all possible promoter configurations. The likelihood
 433 of each configuration was quantified by the transfer function f_{nj} (which we modeled using
 434 Hill like functions), while the lead term in the numerator $W_{R_{1,j}}$ denotes the weight of con-
 435 stitutive expression for gene j . Given this formulation, the rate of constitutive expression
 436 was then given by:

$$\lambda_j = \bar{r}_{T,j} \left(\frac{W_{R_{1,j}}}{1 + W_{R_{1,j}}} \right) \quad (6)$$

437 If a gene expression process had no modifying factors, $u_j = 1$. Lastly, the specific trans-

438 lation rate was modeled as:

$$r_{X,j} = V_X^{max} \left(\frac{L_{X,o}}{L_{X,j}} \right) \left(\frac{m_j}{K_X + m_j} \right) \quad (7)$$

439 where V_X^{max} denotes a characteristic maximum translation rate estimated from literature,
440 and K_X denotes a translation saturation constant. The characteristic maximum translation
441 rate was defined as the product of a characteristic translation rate constant (k_X) and
442 the Ribosome abundance (R_2), $V_X^{max} = k_X (R_2)$. As was the case for transcription, we
443 corrected the characteristic translation rate by the ratio of the length of a characteristic
444 transcription normalized by the length of transcript j .

445 *Signaling model equations.* The signal initiation, and integration modules required the
446 abundance of cRaf-pS621 and ATRA-RXR/RAR (activated Trigger) as inputs. However,
447 our base model described only the abundance of inactive proteins e.g., cRaf or RXR/RAR
448 but not the activated forms. To address this issue, we estimated pseudo steady state
449 approximations for the abundance of cRaf-pS621 and activated Trigger. The abundance
450 of activated trigger ($x_{a,1}$) was estimated directly from the RXR/RAR abundance ($x_{u,1}$):

$$x_{a,1} \sim x_{u,1} \left(\frac{\alpha \cdot \text{ATRA}}{1 + \alpha \cdot \text{ATRA}} \right) \quad (8)$$

451 where α denotes a gain parameter; $\alpha = 0.0$ if ATRA is less than a threshold, and $\alpha = 0.1$
452 if ATRA is greater than the differentiation threshold. The abundance of cRaf-pS621 was
453 estimated by making the pseudo steady state approximation on the cRaf-pS621 balance.
454 The abundance of an activated signaling species i was given by:

$$\frac{dx_i}{dt} = r_{+,i}(\mathbf{x}, \mathbf{k}) - (\mu + k_{d,i}) x_i \quad i = 1, \dots, \mathcal{M} \quad (9)$$

455 The quantity x_i denotes concentration of signaling species i , while \mathcal{R} and \mathcal{M} denote
 456 the number of signaling reactions and signaling species in the model, respectively. The
 457 term $r_{+,i}(\mathbf{x}, \mathbf{k})$ denotes the rate of generation of activated species i , while μ denotes
 458 the specific growth rate, and $k_{d,i}$ denotes the rate constant controlling the non-specific
 459 degradation of x_i . We neglected deactivation reactions e.g., phosphatase activities. We
 460 assumed that signaling processes were fast compared to gene expression; this allowed
 461 us to approximate the signaling balance as:

$$x_i^* \simeq \frac{r_{+,i}(\mathbf{x}, \mathbf{k})}{(\mu + k_{d,i})} \quad i = 1, \dots, \mathcal{M} \quad (10)$$

462 The generation rate was written as the product of a kinetic term ($\bar{r}_{+,i}$) and a control term
 463 (v_i). The control terms $0 \leq v_j \leq 1$ depended upon the combination of factors which in-
 464 fluenced rate process j . If rate j was influenced by $1, \dots, m$ factors, we modeled this
 465 relationship as $v_j = \mathcal{I}_j(f_{1j}(\cdot), \dots, f_{mj}(\cdot))$ where $0 \leq f_{ij}(\cdot) \leq 1$ denotes a regulatory
 466 transfer function quantifying the influence of factor i on rate j . The function $\mathcal{I}_j(\cdot)$ is an
 467 integration rule which maps the output of regulatory transfer functions into a control vari-
 468 able. In this study, we used $\mathcal{I}_j \in \{\min, \max\}$ and hill transfer functions (54). If a process
 469 had no modifying factors, $v_j = 1$. The kinetic rate of cRaf-pS621 generation $\bar{r}_{+,cRaf}$ was
 470 modeled as:

$$\bar{r}_{+,cRaf} = k_{+,cRaf} x_s \left(\frac{x_{cRaf}}{K_{+,cRaf} + x_{cRaf}} \right) \quad (11)$$

471 where x_s denotes the signalsome abundance, and $K_{+,cRaf}$ denotes a saturation constant
 472 governing cRaf-pS621 formation. The formation of cRaf-pS621 was regulated by only a
 473 single factor, the abundance of MAPK inhibitor, thus $v_{+,cRaf}$ took the form:

$$v_{+,cRaf} = \left(1 - \frac{I}{K_D + I} \right) \quad (12)$$

474 where I denotes the abundance of the MAPK inhibitor, and K_D denotes the inhibitor
475 affinity.

476 *Estimation of gene expression model parameters.* We estimated parameters appearing
477 in the mRNA and protein balances, the abundance of polymerases and ribosomes, tran-
478 scription and translation rates, the half-life of a typical mRNA and protein, and typical
479 values for the copies per cell of RNA polymerase and ribosomes from literature (Table 2).
480 The saturation constants K_X and K_T were adjusted so that gene expression and trans-
481 lation resulted in gene products on a biologically realistic concentration scale. Lastly, we
482 calculated the concentration for gene G_j by assuming, on average, that a cell had two
483 copies of each gene at any given time. Thus, the bulk of our gene expression model pa-
484 rameters were based directly upon literature values, and were not adjusted during model
485 identification. However, the remaining parameters, e.g., the W_{ij} appearing in the gene
486 expression control laws, or parameters appearing in the transfer functions f_{dij} , were esti-
487 mated from the protein expression and signaling data sets discussed here.

488 Signaling and gene expression model parameters were estimated by minimizing the
489 squared difference between simulations and experimental protein data set j . We mea-
490 sured the squared difference in the scale, fold change and shape for protein j :

$$E_j(\mathbf{k}) = \left(\mathcal{M}_j(t_-) - \hat{y}_j(t_-, \mathbf{k}) \right)^2 + \sum_{i=1}^{\mathcal{T}_j} \left(\hat{\mathcal{M}}_{ij} - \hat{y}_{ij}(\mathbf{k}) \right)^2 + \sum_{i=1}^{\mathcal{T}_j} \left(\mathcal{M}'_{ij} - y'_{ij}(\mathbf{k}) \right)^2 \quad (13)$$

491 The first term in Eq. (13) quantified the initial *scale* error, directly before the addition
492 of ATRA. In this case, $\mathcal{M}_j(t_-)$ (the approximate concentration of protein j before the
493 addition of ATRA) was estimated from literature. This term was required because the
494 protein measurements were reported as the fold-change; thus, the data was normalized
495 by a control value measured before the addition of ATRA. However, the model operated on
496 a physical scale. The first term allowed the model to capture physically realistic changes

497 following ATRA addition. The second term quantified the difference in the *fold-change* of
 498 protein j as a function of time. The terms $\hat{\mathcal{M}}_{ij}$ and \hat{y}_{ij} denote the scaled experimental
 499 observations and simulation outputs (fold-change; protein normalized by control value
 500 directly before ATRA addition) at time i from protein j , where T_j denoted the number of
 501 time points for data set j . Lastly, the third term of the objective function measured the
 502 difference in the *shape* of the measured and simulated protein levels. The scaled value
 503 $0 \leq \mathcal{M}'_{ij} \leq 1$ was given by:

$$\hat{\mathcal{M}}_{ij} = \left(\mathcal{M}_{ij} - \min_i \mathcal{M}_{ij} \right) / \left(\max_i \mathcal{M}_{ij} - \min_i \mathcal{M}_{ij} \right) \quad (14)$$

504 where $\mathcal{M}'_{ij} = 0$ and $\mathcal{M}'_{ij} = 1$ describe the lowest (highest) intensity bands. A similar
 505 scaling was used for the simulation output. We minimized the total model residual $\sum_j E_j$
 506 using a heuristic direct-search optimization procedure, subject to box constraints on the
 507 parameter values, starting from a random initial parameter guess. Each downhill step was
 508 archived and used for ensemble calculations. The optimization procedure (a covariance
 509 matrix adaptation evolution strategy) has been reported previously (55).

510 *Estimation of an effective cell cycle arrest model.* We formulated an effective N-order
 511 polynomial model of the fraction of cells undergoing ATRA-induced cell cycle arrest at
 512 time t , $\hat{\mathcal{A}}(t)$, as:

$$\hat{\mathcal{A}}(t) \simeq a_0 + \sum_{i=1}^{N-1} a_i \phi_i(\mathbf{p}(t), t) \quad (15)$$

513 where a_i were unknown parameters, and $\phi_i(\mathbf{p}(t), t)$ denotes a basis function. The basis
 514 functions were dependent upon the system state; in this study, we assumed $N = 4$ and
 515 basis functions of the form:

$$\phi_i(\mathbf{p}(t), t) = \left(\frac{t}{T} + \frac{p21}{E2F} \Big|_t \right)^{(i-1)} \quad (16)$$

516 The parameters a_0, \dots, a_3 were estimated directly from cell-cycle measurements (biologi-
517 cal replicates) using least-squares.

518 *Availability of model code.* The signaling and gene expression model equations, and the
519 parameter estimation procedure, were implemented in the Julia programming language.
520 The model equations were solved using the ODE23s routine of the ODE package (56). The
521 model code and parameter ensemble is freely available under an MIT software license
522 and can be downloaded from <http://www.varnerlab.org>.

523 *Cell culture and treatment* Human myeloblastic leukemia cells (HL-60 cells) were grown
524 in a humidified atmosphere of 5% CO₂ at 37°C and maintained in RPMI 1640 from Gibco
525 (Carlsbad, CA) supplemented with 5% heat inactivated fetal bovine serum from Hyclone
526 (Logan, UT) and 1× antibiotic/antimicotic (Gibco, Carlsbad, CA). Cells were cultured in
527 constant exponential growth (57). Experimental cultures were initiated at 0.1×10^6 cells/mL
528 24 hr prior to ATRA treatment; if indicated, cells were also treated with GW5074 (2 μ M) 18
529 hr before ATRA treatment. For the cell culture washout experiments, cells were treated
530 with ATRA for 24 hr, washed 3x with prewarmed serum supplemented culture medium
531 to remove ATRA, and reseeded in ATRA-free media as described. Western blot analysis
532 was performed at incremental time points after removal of ATRA.

533 *Chemicals* All-Trans Retinoic Acid (ATRA) from Sigma-Aldrich (St. Louis, MO) was dis-
534 solved in 100% ethanol with a stock concentration of 5mM, and used at a final concen-
535 tration of 1 μ M (unless otherwise noted). The cRaf inhibitor GW5074 from Sigma-Aldrich
536 (St. Louis, MO) was dissolved in DMSO with a stock concentration of 10mM, and used
537 at a final concentration of 2 μ M. HL-60 cells were treated with 2 μ M GW5074 with or with-
538 out ATRA (1 μ M) at 0 hr. This GW5074 dosage had a negligible effect on the cell cycle
539 distribution, compared to ATRA treatment alone.

540 *Immunoprecipitation and western blotting* Approximately 1.2×10^7 cells were lysed using
541 $400\mu\text{L}$ of M-Per lysis buffer from Thermo Scientific (Waltham, MA). Lysates were cleared
542 by centrifugation at $16,950 \times g$ in a micro-centrifuge for 20 min at 4°C . Lysates were
543 pre-cleared using $100\mu\text{L}$ protein A/G Plus agarose beads from Santa Cruz Biotechnology
544 (Santa Cruz, CA) by inverting overnight at 4°C . Beads were cleared by centrifugation and
545 total protein concentration was determined by a BCA assay (Thermo Scientific, Waltham,
546 MA). Immunoprecipitations were setup by bringing lysate to a concentration of 1g/L in a
547 total volume of $300\mu\text{L}$ (M-Per buffer was used for dilution). The anti-Raf antibody was
548 added at $3\mu\text{L}$. A negative control with no bait protein was also used to exclude the di-
549 rect interaction of proteins with the A/G beads. After 1 hr of inversion at 4°C , $20\mu\text{L}$ of
550 agarose beads was added and samples were left to invert overnight at 4°C . Samples
551 were then washed three times with M-Per buffer by centrifugation. Finally proteins were
552 eluted from agarose beads using a laemmli loading buffer. Eluted proteins were resolved
553 by SDS-PAGE and Western blotting. Total lysate samples were normalized by total protein
554 concentration ($20\mu\text{g}$ per sample) and resolved by SDS-PAGE and Western blotting. Sec-
555 ondary HRP bound antibody was used for visualization. All antibodies were purchased
556 from Cell Signaling (Boston, MA) with the exception of α -p621 Raf which was purchased
557 from Biosource/Invitrogen (Carlsbad, CA), and α -CK2 from BD Biosciences (San Jose,
558 CA).

559 *Morphology assessment* Untreated and ATRA-treated HL-60 cells were collected after
560 72 hr and cytocentrifuged for 3 min at 700 rpm onto glass slides. Slides were air-dried
561 and stained with Wright's stain. Slide images were captured at 40X (Leica DM LB 100T
562 microscope, Leica Microsystems).

563 **Competing interests**

564 The authors declare that they have no competing interests.

565 **Author's contributions**

566 J.V and A.Y directed the study. R.T, H.J, R.B and J.C conducted the cell culture measure-
567 ments. J.V, R.B, W.D, K.R and A.S developed the reduced order HL-60 models and the
568 parameter ensemble. W.D and J.V analyzed the model ensemble, and generated figures
569 for the manuscript. The manuscript was prepared and edited for publication by W.D, A.Y
570 and J.V.

571 **Acknowledgements**

572 We gratefully acknowledge the suggestions from the anonymous reviewers to improve
573 this manuscript.

574 **Funding**

575 We acknowledge the financial support to J.V. by the National Science Foundation CA-
576 REER (CBET-0846876) for the support of R.T. and H.J. In addition, we acknowledge
577 support to A.Y. from the National Institutes of Health (CA 30555, CA152870) and a grant
578 from New York State Stem Cell Science. Lastly, we acknowledge the financial support to
579 J.V. and A.Y. from the National Cancer Institute (#U54 CA143876). The content is solely
580 the responsibility of the authors and does not necessarily represent the official views of
581 the National Cancer Institute or the National Institutes of Health.

582 **References**

- 583 1. Bushue N, Wan YJY (2010) Retinoid pathway and cancer therapeutics. *Adv Drug
584 Deliv Rev* 62: 1285-98.
- 585 2. Tang XH, Gudas LJ (2011) Retinoids, retinoic acid receptors, and cancer. *Annu Rev
586 Pathol* 6: 345-64.
- 587 3. Cheung FSG, Lovicu FJ, Reichardt JKV (2012) Current progress in using vitamin d
588 and its analogs for cancer prevention and treatment. *Expert Rev Anticancer Ther*
589 12: 811-37.
- 590 4. Nilsson B (1984) Probable in vivo induction of differentiation by retinoic acid of
591 promyelocytes in acute promyelocytic leukaemia. *Br J Haematol* 57: 365-71.
- 592 5. Warrell RP Jr (1993) Retinoid resistance in acute promyelocytic leukemia: new
593 mechanisms, strategies, and implications. *Blood* 82: 1949-53.
- 594 6. Freemantle SJ, Spinella MJ, Dmitrovsky E (2003) Retinoids in cancer therapy and
595 chemoprevention: promise meets resistance. *Oncogene* 22: 7305-15.
- 596 7. Breitman TR, Selonick SE, Collins SJ (1980) Induction of differentiation of the hu-
597 man promyelocytic leukemia cell line (HL-60) by retinoic acid. *Proc Natl Acad Sci U
598 S A* 77: 2936–2940.
- 599 8. Yen A, Roberson MS, Varvayanis S, Lee AT (1998) Retinoic acid induced
600 mitogen-activated protein (MAP)/extracellular signal-regulated kinase (ERK) kinase-
601 dependent MAP kinase activation needed to elicit HL-60 cell differentiation and
602 growth arrest. *Cancer Res* 58: 3163–3172.
- 603 9. Hong HY, Varvayanis S, Yen A (2001) Retinoic acid causes MEK-dependent RAF
604 phosphorylation through RARalpha plus RXR activation in HL-60 cells. *Differentia-
605 tion* 68: 55–66.
- 606 10. Mangelsdorf DJ, Ong ES, Dyck JA, Evans RM (1990) Nuclear receptor that identifies
607 a novel retinoic acid response pathway. *Nature* 345: 224–229.

- 608 11. Congleton J, MacDonald R, Yen A (2012) Src inhibitors, PP2 and dasatinib, increase
609 retinoic acid-induced association of Lyn and c-Raf (S259) and enhance MAPK-
610 dependent differentiation of myeloid leukemia cells. Leukemia 26: 1180-8.
- 611 12. Shen M, Bunaci R, Congleton J, Jensen H, Sayam L, et al. (2011) Interferon regu-
612 latory factor-1 binds c-Cbl, enhances mitogen activated protein kinase signaling and
613 promotes retinoic acid-induced differentiation of HL-60 human myelo-monoblastic
614 leukemia cells. Leuk Lymphoma 52: 2372-9.
- 615 13. Shen M, Yen A (2009) c-Cbl tyrosine kinase-binding domain mutant G306E abol-
616 ishes the interaction of c-Cbl with CD38 and fails to promote retinoic acid-induced
617 cell differentiation and G0 arrest. J Biol Chem 284: 25664–25677.
- 618 14. Yen A, Varvayanis S, Smith J, Lamkin T (2006) Retinoic acid induces expression of
619 SLP-76: expression with c-FMS enhances ERK activation and retinoic acid-induced
620 differentiation/G0 arrest of HL-60 cells. Eur J Cell Biol 85: 117–132.
- 621 15. Marchisio M, Bertagnolo V, Colamussi ML, Capitani S, Neri LM (1998) Phos-
622 phatidylinositol 3-kinase in HL-60 nuclei is bound to the nuclear matrix and increases
623 during granulocytic differentiation. Biochem Biophys Res Commun 253: 346-51.
- 624 16. Congleton J, Jiang H, Malavasi F, Lin H, Yen A (2011) ATRA-induced HL-60 myeloid
625 leukemia cell differentiation depends on the CD38 cytosolic tail needed for mem-
626 brane localization, but CD38 enzymatic activity is unnecessary. Exp Cell Res 317:
627 910–919.
- 628 17. Wang J, Yen A (2004) A novel retinoic acid-responsive element regulates retinoic
629 acid induced BLR1 expression. Mol Cell Biol 24: 2423 - 2443.
- 630 18. Yen A (1990) HL-60 cells as a model of growth and differentiation: the significance
631 of variant cells. Hematology Review 4: 5-46.
- 632 19. Yang T, Xiong Q, Enslen H, Davis R, Chow CW (2002) Phosphorylation of NFATc4
633 by p38 mitogen-activated protein kinases. Mol Cell Biol 22: 3892–3904.

- 634 20. Wang J, Yen A (2008) A MAPK-positive Feedback Mechanism for BLR1 Signaling
635 Propels Retinoic Acid-triggered Differentiation and Cell Cycle Arrest. *J Biol Chem*
636 283: 4375–4386.
- 637 21. Tasseff R, Nayak S, Song S, Yen A, Varner J (2011) Modeling and analysis of retinoic
638 acid induced differentiation of uncommitted precursor cells. *Integr Biol* 3: 578 - 591.
- 639 22. Jensen HA, Styskal LE, Tasseff R, Bunaciu RP, Congleton J, et al. (2013) The
640 src-family kinase inhibitor pp2 rescues inducible differentiation events in emergent
641 retinoic acid-resistant myeloblastic leukemia cells. *PLoS One* 8: e58621.
- 642 23. Jensen HA, Bunaciu RP, Ibabao CN, Myers R, Varner JD, et al. (2014) Retinoic acid
643 therapy resistance progresses from unilineage to bilineage in hl-60 leukemic blasts.
644 *PLoS One* 9: e98929.
- 645 24. Jensen HA, Bunaciu RP, Varner JD, Yen A (2015) Gw5074 and pp2 kinase inhibitors
646 implicate nontraditional c-raf and lyn function as drivers of retinoic acid-induced mat-
647 uration. *Cell Signal* 27: 1666-75.
- 648 25. Jensen HA, Yourish HB, Bunaciu RP, Varner JD, Yen A (2015) Induced myelomono-
649 cytic differentiation in leukemia cells is accompanied by noncanonical transcription
650 factor expression. *FEBS Open Bio* 5: 789-800.
- 651 26. Milo R, Jorgensen P, Moran U, Weber G, Springer M (2010) Bionumbers—the
652 database of key numbers in molecular and cell biology. *Nucleic Acids Res* 38: D750-
653 3.
- 654 27. Katagiri K, Hattori S, Nakamura S, Yamamoto T, Yoshida T, et al. (1994) Activation
655 of ras and formation of gap complex during tpa-induced monocytic differentiation of
656 hl-60 cells. *Blood* 84: 1780–1789.
- 657 28. Miranda MB, Johnson DE (2007) Signal transduction pathways that contribute to
658 myeloid differentiation. *Leukemia* 21: 1363–1377.
- 659 29. Hickstein DD, Back AL, Collins SJ (1989) Regulation of expression of the cd11b and

- 660 cd18 subunits of the neutrophil adherence receptor during human myeloid differen-
661 tiation. *J Biol Chem* 264: 21812–21817.
- 662 30. Hornstein I, Alcover A, Katzav S (2004) Vav proteins, masters of the world of cy-
663 toskeleton organization. *Cell Signal* 16: 1-11.
- 664 31. Ferrell J (2002) Self-perpetuating states in signal transduction: positive feedback,
665 double-negative feedback and bistability. *Curr Opin Cell Biol* 14: 140-8.
- 666 32. Laslo P, Spooner CJ, Warmflash A, Lancki DW, Lee HJ, et al. (2006) Multilineage
667 transcriptional priming and determination of alternate hematopoietic cell fates. *Cell*
668 126: 755-66.
- 669 33. Xiong W, Ferrell J (2003) A positive-feedback-based bistable 'memory module' that
670 governs a cell fate decision. *Nature* 426: 460-5.
- 671 34. Bagci EZ, Vodovotz Y, Billiar TR, Ermentrout GB, Bahar I (2006) Bistability in apop-
672 tosis: roles of bax, bcl-2, and mitochondrial permeability transition pores. *Biophys J*
673 90: 1546-59.
- 674 35. Luan D, Zai M, Varner JD (2007) Computationally derived points of fragility of a
675 human cascade are consistent with current therapeutic strategies. *PLoS Comput
676 Biol* 3: e142.
- 677 36. Friedman AD (2007) Transcriptional control of granulocyte and monocyte develop-
678 ment. *Oncogene* 26: 6816-28.
- 679 37. Dahl R, Walsh JC, Lancki D, Laslo P, Iyer SR, et al. (2003) Regulation of macrophage
680 and neutrophil cell fates by the PU.1:C/EBPalpha ratio and granulocyte colony-
681 stimulating factor. *Nat Immunol* 4: 1029-36.
- 682 38. El-Benna J, Dang PMC, Gougerot-Pocidalo MA, Marie JC, Braut-Boucher F (2009)
683 p47phox, the phagocyte nadph oxidase/nox2 organizer: structure, phosphorylation
684 and implication in diseases. *Exp Mol Med* 41: 217-25.
- 685 39. Hock H, Hamblen MJ, Rooke HM, Traver D, Bronson RT, et al. (2003) Intrinsic re-

- 686 requirement for zinc finger transcription factor gfi-1 in neutrophil differentiation. Immuno-
687 nity 18: 109-20.
- 688 40. Cleghon V, Morrison DK (1994) Raf-1 interacts with fyn and src in a non-
689 phosphotyrosine-dependent manner. J Biol Chem 269: 17749–17755.
- 690 41. Zimmermann S, Moelling K (1999) Phosphorylation and regulation of raf by akt (pro-
691 tein kinase b). Science 286: 1741–1744.
- 692 42. Ritt DA, Zhou M, Conrads TP, Veenstra TD, Copeland TD, et al. (2007) Ck2 is a
693 component of the ksr1 scaffold complex that contributes to raf kinase activation.
694 Curr Biol 17: 179–184.
- 695 43. Hekman M, Wiese S, Metz R, Albert S, Troppmair J, et al. (2004) Dynamic changes
696 in c-raf phosphorylation and 14-3-3 protein binding in response to growth factor stim-
697 ulation: differential roles of 14-3-3 protein binding sites. J Biol Chem 279: 14074–
698 14086.
- 699 44. Dhillon AS, Yip YY, Grindlay GJ, Pakay JL, Dangers M, et al. (2009) The c-terminus
700 of raf-1 acts as a 14-3-3-dependent activation switch. Cell Signal 21: 1645–1651.
- 701 45. Song JS, Gomez J, Stancato LF, Rivera J (1996) Association of a p95 vav-containing
702 signaling complex with the fcepsiloniori gamma chain in the rbl-2h3 mast cell line.
703 evidence for a constitutive in vivo association of vav with grb2, raf-1, and erk2 in an
704 active complex. J Biol Chem 271: 26962–26970.
- 705 46. Costello PS, Walters AE, Mee PJ, Turner M, Reynolds LF, et al. (1999) The rho-
706 family gtp exchange factor vav is a critical transducer of t cell receptor signals to the
707 calcium, erk, and nf-kappab pathways. Proc Natl Acad Sci U S A 96: 3035–3040.
- 708 47. Graham D, Robertson C, Bautista J, Mascarenhas F, Diacovo M, et al. (2007)
709 Neutrophil-mediated oxidative burst and host defense are controlled by a Vav-
710 PLCgamma2 signaling axis in mice. J Clin Invest 117: 3445–3452.
- 711 48. Kim HS, Lim IK (2009) Phosphorylated extracellular signal-regulated protein kinases

- 712 1 and 2 phosphorylate sp1 on serine 59 and regulate cellular senescence via tran-
713 scription of p21sdi1/cip1/waf1. *J Biol Chem* 284: 15475–15486.
- 714 49. Milanini-Mongiat J, Pouyss?gur J, Pag?s G (2002) Identification of two sp1 phos-
715 phorylation sites for p42/p44 mitogen-activated protein kinases: their implication in
716 vascular endothelial growth factor gene transcription. *J Biol Chem* 277: 20631–
717 20639.
- 718 50. Zhang Y, Cho YY, Petersen BL, Zhu F, Dong Z (2004) Evidence of stat1 phosphor-
719 ylation modulated by mapks, mek1 and msk1. *Carcinogenesis* 25: 1165–1175.
- 720 51. Li Z, Theus MH, Wei L (2006) Role of erk 1/2 signaling in neuronal differentiation of
721 cultured embryonic stem cells. *Dev Growth Differ* 48: 513–523.
- 722 52. Yen A, Reece SL, Albright KL (1984) Dependence of hl-60 myeloid cell differentiation
723 on continuous and split retinoic acid exposures: precommitment memory associated
724 with altered nuclear structure. *J Cell Physiol* 118: 277–286.
- 725 53. Moon TS, Lou C, Tamsir A, Stanton BC, Voigt CA (2012) Genetic programs con-
726 structed from layered logic gates in single cells. *Nature* 491: 249-53.
- 727 54. Wayman JA, Sagar A, Varner JD (2015) Dynamic modeling of cell-free biochemical
728 networks using effective kinetic models. *Processes* 3: 138.
- 729 55. Igel C, Hansen N, Roth S (2007) Covariance matrix adaptation for multi-objective
730 optimization. *Evol Comput* 15: 1-28.
- 731 56. Bezanson J, Edelman A, Karpinski S, Shah VB (2014) Julia: A fresh approach to
732 numerical computing. *CoRR* abs/1411.1607.
- 733 57. Brooks SC, Kazmer S, Levin AA, Yen A (1996) Myeloid differentiation and retinoblas-
734 toma phosphorylation changes in HL-60 cells induced by retinoic acid receptor- and
735 retinoid X receptor-selective retinoic acid analogs. *Blood* 87: 227–237.
- 736 58. Rishi AK, Gerald TM, Shao ZM, Li XS, Baumann RG, et al. (1996) Regulation of the
737 human retinoic acid receptor alpha gene in the estrogen receptor negative human

- 738 breast carcinoma cell lines skbr-3 and mda-mb-435. Cancer Res 56: 5246-52.

739 59. Mueller BU, Pabst T, Fos J, Petkovic V, Fey MF, et al. (2006) Atra resolves the dif-
740 ferentiation block in t(15;17) acute myeloid leukemia by restoring pu.1 expression.
741 Blood 107: 3330-8.

742 60. Luo XM, Ross AC (2006) Retinoic acid exerts dual regulatory actions on the ex-
743 pression and nuclear localization of interferon regulatory factor-1. Exp Biol Med
744 (Maywood) 231: 619-31.

745 61. Sylvester I, Schöler HR (1994) Regulation of the oct-4 gene by nuclear receptors.
746 Nucleic Acids Res 22: 901-11.

747 62. Drach J, McQueen T, Engel H, Andreeff M, Robertson KA, et al. (1994) Retinoic
748 acid-induced expression of cd38 antigen in myeloid cells is mediated through
749 retinoic acid receptor-alpha. Cancer Res 54: 1746-52.

750 63. Liu M, Iavarone A, Freedman LP (1996) Transcriptional activation of the human
751 p21(waf1/cip1) gene by retinoic acid receptor. correlation with retinoid induction of
752 u937 cell differentiation. J Biol Chem 271: 31723-8.

753 64. Bunaciu RP, Yen A (2013) 6-formylindolo (3,2-b)carbazole (ficz) enhances retinoic
754 acid (ra)-induced differentiation of hl-60 myeloblastic leukemia cells. Mol Cancer 12:
755 39.

756 65. Balmer JE, Blomhoff R (2002) Gene expression regulation by retinoic acid. J Lipid
757 Res 43: 1773-808.

758 66. Rosen ED, Hsu CH, Wang X, Sakai S, Freeman MW, et al. (2002) C/ebpalpha in-
759 duces adipogenesis through ppargamma: a unified pathway. Genes Dev 16: 22-6.

760 67. Varley CL, Bacon EJ, Holder JC, Southgate J (2009) Foxa1 and irf-1 intermediary
761 transcriptional regulators of ppargamma-induced urothelial cytodifferentiation. Cell
762 Death Differ 16: 103-14.

763 68. Bruemmer D, Yin F, Liu J, Berger JP, Sakai T, et al. (2003) Regulation of the growth

- 764 arrest and dna damage-inducible gene 45 (gadd45) by peroxisome proliferator-
765 activated receptor gamma in vascular smooth muscle cells. Circ Res 93: e38-47.
- 766 69. Delerive P, De Bosscher K, Besnard S, Vanden Berghe W, Peters JM, et al. (1999)
767 Peroxisome proliferator-activated receptor alpha negatively regulates the vascular
768 inflammatory gene response by negative cross-talk with transcription factors nf-
769 kappaB and ap-1. J Biol Chem 274: 32048-54.
- 770 70. Altiok S, Xu M, Spiegelman BM (1997) Ppargamma induces cell cycle withdrawal:
771 inhibition of e2f/dp dna-binding activity via down-regulation of pp2a. Genes Dev 11:
772 1987-98.
- 773 71. Fei J, Cook C, Gillespie M, Yu B, Fullen K, et al. (2011) Atherogenic ω -6 lipids mod-
774 ulate ppar- egr-1 crosstalk in vascular cells. PPAR Res 2011: 753917.
- 775 72. Song EK, Lee YR, Kim YR, Yeom JH, Yoo CH, et al. (2012) Naadp mediates insulin-
776 stimulated glucose uptake and insulin sensitization by ppar γ in adipocytes. Cell Rep
777 2: 1607-19.
- 778 73. Szanto A, Nagy L (2005) Retinoids potentiate peroxisome proliferator-activated re-
779 ceptor gamma action in differentiation, gene expression, and lipid metabolic pro-
780 cesses in developing myeloid cells. Mol Pharmacol 67: 1935-43.
- 781 74. Han S, Sidell N, Fisher PB, Roman J (2004) Up-regulation of p21 gene expres-
782 sion by peroxisome proliferator-activated receptor gamma in human lung carcinoma
783 cells. Clin Cancer Res 10: 1911-9.
- 784 75. Von Knethen A, Brüne B (2002) Activation of peroxisome proliferator-activated re-
785 ceptor gamma by nitric oxide in monocytes/macrophages down-regulates p47phox
786 and attenuates the respiratory burst. J Immunol 169: 2619-26.
- 787 76. Dispirito JR, Fang B, Wang F, Lazar MA (2013) Pruning of the adipocyte peroxisome
788 proliferator-activated receptor γ cistrome by hematopoietic master regulator pu.1.
789 Mol Cell Biol 33: 3354-64.

- 790 77. Chen H, Ray-Gallet D, Zhang P, Hetherington CJ, Gonzalez DA, et al. (1995) Pu.1
791 (spi-1) autoregulates its expression in myeloid cells. *Oncogene* 11: 1549-60.
- 792 78. Steidl U, Rosenbauer F, Verhaak RGW, Gu X, Ebralidze A, et al. (2006) Essential
793 role of jun family transcription factors in pu.1 knockdown-induced leukemic stem
794 cells. *Nat Genet* 38: 1269-77.
- 795 79. Pahl HL, Scheibe RJ, Zhang DE, Chen HM, Galson DL, et al. (1993) The proto-
796 oncogene pu.1 regulates expression of the myeloid-specific cd11b promoter. *J Biol
797 Chem* 268: 5014-20.
- 798 80. Yuki H, Ueno S, Tatetsu H, Niiro H, Iino T, et al. (2013) Pu.1 is a potent tumor
799 suppressor in classical hodgkin lymphoma cells. *Blood* 121: 962-70.
- 800 81. Li SL, Schlegel W, Valente AJ, Clark RA (1999) Critical flanking sequences of pu.1
801 binding sites in myeloid-specific promoters. *J Biol Chem* 274: 32453-60.
- 802 82. Timchenko N, Wilson DR, Taylor LR, Abdelsayed S, Wilde M, et al. (1995) Autoreg-
803 ulation of the human c/ebp alpha gene by stimulation of upstream stimulatory factor
804 binding. *Mol Cell Biol* 15: 1192-202.
- 805 83. Lidonnici MR, Audia A, Soliera AR, Prisco M, Ferrari-Amorotti G, et al. (2010) Ex-
806 pression of the transcriptional repressor gfi-1 is regulated by c/ebpalpha and is
807 involved in its proliferation and colony formation-inhibitory effects in p210bcr/abl-
808 expressing cells. *Cancer Res* 70: 7949-59.
- 809 84. D'Alo' F, Johansen LM, Nelson EA, Radomska HS, Evans EK, et al. (2003) The
810 amino terminal and e2f interaction domains are critical for c/ebp alpha-mediated
811 induction of granulopoietic development of hematopoietic cells. *Blood* 102: 3163-
812 71.
- 813 85. Pan Z, Hetherington CJ, Zhang DE (1999) Ccaat/enhancer-binding protein activates
814 the cd14 promoter and mediates transforming growth factor beta signaling in mono-
815 cyte development. *J Biol Chem* 274: 23242-8.

- 816 86. Harris TE, Albrecht JH, Nakanishi M, Darlington GJ (2001) Ccaat/enhancer-binding
817 protein-alpha cooperates with p21 to inhibit cyclin-dependent kinase-2 activity and
818 induces growth arrest independent of dna binding. *J Biol Chem* 276: 29200-9.
- 819 87. Bauvois B, Durant L, Laboureau J, Barthélémy E, Rouillard D, et al. (1999) Upreg-
820 ulation of cd38 gene expression in leukemic b cells by interferon types i and ii. *J*
821 *Interferon Cytokine Res* 19: 1059-66.
- 822 88. Passioura T, Dolnikov A, Shen S, Symonds G (2005) N-ras-induced growth suppres-
823 sion of myeloid cells is mediated by irf-1. *Cancer Res* 65: 797-804.
- 824 89. Dahl R, Iyer SR, Owens KS, Cuylear DD, Simon MC (2007) The transcriptional
825 repressor gfi-1 antagonizes pu.1 activity through protein-protein interaction. *J Biol*
826 *Chem* 282: 6473-83.
- 827 90. Duan Z, Horwitz M (2003) Targets of the transcriptional repressor oncoprotein gfi-1.
828 *Proc Natl Acad Sci U S A* 100: 5932-7.
- 829 91. Chen H, Zhang P, Radomska HS, Hetherington CJ, Zhang DE, et al. (1996) Octamer
830 binding factors and their coactivator can activate the murine pu.1 (spi-1) promoter.
831 *J Biol Chem* 271: 15743-52.
- 832 92. Behre G, Whitmarsh AJ, Coghlan MP, Hoang T, Carpenter CL, et al. (1999) c-jun
833 is a jnk-independent coactivator of the pu.1 transcription factor. *J Biol Chem* 274:
834 4939-46.
- 835 93. Kardassis D, Papakosta P, Pardali K, Moustakas A (1999) c-jun transactivates the
836 promoter of the human p21(waf1/cip1) gene by acting as a superactivator of the
837 ubiquitous transcription factor sp1. *J Biol Chem* 274: 29572-81.
- 838 94. Johnson DG, Ohtani K, Nevins JR (1994) Autoregulatory control of e2f1 expression
839 in response to positive and negative regulators of cell cycle progression. *Genes Dev*
840 8: 1514-25.
- 841 95. Fu M, Zhang J, Lin Y, Zhu X, Ehrengruber MU, et al. (2002) Early growth response

- 842 factor-1 is a critical transcriptional mediator of peroxisome proliferator-activated
843 receptor-gamma 1 gene expression in human aortic smooth muscle cells. J Biol
844 Chem 277: 26808-14.
- 845 96. Mak KS, Funnell APW, Pearson RCM, Crossley M (2011) Pu.1 and haematopoietic
846 cell fate: Dosage matters. Int J Cell Biol 2011: 808524.
- 847 97. Chen F, Wang Q, Wang X, Studzinski GP (2004) Up-regulation of egr1 by 1,25-
848 dihydroxyvitamin d3 contributes to increased expression of p35 activator of cyclin-
849 dependent kinase 5 and consequent onset of the terminal phase of hl60 cell differ-
850 entiation. Cancer Res 64: 5425-33.
- 851 98. Suh J, Jeon YJ, Kim HM, Kang JS, Kaminski NE, et al. (2002) Aryl hydrocarbon
852 receptor-dependent inhibition of ap-1 activity by 2,3,7,8-tetrachlorodibenzo-p-dioxin
853 in activated b cells. Toxicol Appl Pharmacol 181: 116-23.
- 854 99. Shen M, Bunaciu RP, Congleton J, Jensen HA, Sayam LG, et al. (2011) Inter-
855 feron regulatory factor-1 binds c-cbl, enhances mitogen activated protein kinase
856 signaling and promotes retinoic acid-induced differentiation of hl-60 human myelo-
857 monoblastic leukemia cells. Leuk Lymphoma 52: 2372-9.
- 858 100. Bunaciu RP, Yen A (2011) Activation of the aryl hydrocarbon receptor ahr promotes
859 retinoic acid-induced differentiation of myeloblastic leukemia cells by restricting ex-
860 pression of the stem cell transcription factor oct4. Cancer Res 71: 2371-80.
- 861 101. Jackson DA, Pombo A, Iborra F (2000) The balance sheet for transcription: an anal-
862 ysis of nuclear rna metabolism in mammalian cells. FASEB J 14: 242-54.
- 863 102. Zhao ZW, Roy R, Gebhardt JCM, Suter DM, Chapman AR, et al. (2014) Spatial orga-
864 nization of rna polymerase ii inside a mammalian cell nucleus revealed by reflected
865 light-sheet superresolution microscopy. Proc Natl Acad Sci U S A 111: 681-6.
- 866 103. Freitas R, Merkle R (2004) Kinematic Self-Replicating Machines. Oxford University
867 Press.

- 868 104. Yang E, van Nimwegen E, Zavolan M, Rajewsky N, Schroeder M, et al. (2003) Decay rates of human mRNAs: correlation with functional characteristics and sequence
869 attributes. *Genome Res* 13: 1863-72.
- 870
- 871 105. Doherty MK, Hammond DE, Clague MJ, Gaskell SJ, Beynon RJ (2009) Turnover
872 of the human proteome: determination of protein intracellular stability by dynamic
873 SILAC. *J Proteome Res* 8: 104-12.
- 874
- 875 106. Sehgal PB, Derman E, Molloy GR, Tamm I, Darnell JE (1976) 5,6-dichloro-1-beta-
876 d-ribofuranosylbenzimidazole inhibits initiation of nuclear heterogeneous RNA chains
in HeLa cells. *Science* 194: 431-3.
- 877
- 878 107. Darzacq X, Shav-Tal Y, de Turris V, Brody Y, Shenoy SM, et al. (2007) In vivo dynamics of RNA polymerase II transcription. *Nat Struct Mol Biol* 14: 796-806.
- 879
- 880 108. Kos M, Tollervey D (2010) Yeast pre-rRNA processing and modification occur cotranscriptionally. *Mol Cell* 37: 809-20.
- 881
- 882 109. Darnell JE Jr (2013) Reflections on the history of pre-mRNA processing and highlights
of current knowledge: a unified picture. *RNA* 19: 443-60.
- 883
- 884 110. Boström K, Wettsten M, Borén J, Bondjers G, Wiklund O, et al. (1986) Pulse-chase
885 studies of the synthesis and intracellular transport of apolipoprotein B-100 in Hep G2
cells. *J Biol Chem* 261: 13800-6.
- 886
- 887 111. Meyers R, editor (2004) *Encyclopedia of Molecular Cell Biology and Molecular
Medicine*, Volume 1, 2nd Edition. ISBN: 978-3-527-30543-8. Wiley-Blackwell.
- 888
- 889 112. Rosenbluth MJ, Lam WA, Fletcher DA (2006) Force microscopy of nonadherent
cells: a comparison of leukemia cell deformability. *Biophys J* 90: 2994-3003.
- 890
- 891 113. O'Leary NA, Wright MW, Brister JR, Ciufo S, Haddad D, et al. (2016) Reference
sequence (RefSeq) database at NCBI: current status, taxonomic expansion, and functional
annotation. *Nucleic Acids Res* 44: D733-45.
- 892

Table 1: Myelomonocytic transcription factor connectivity used in the signal integration and phenotype modules.

Effector	Effect	Target	Source
RAR α	+	RAR α	(58)
	+	PU.1	(59)
	+	C/EBP α	(36)
	+	IRF-1	(60)
	-	Oct4	(61)
	+	CD38	(62)
	+	p21	(63)
	+	AhR	(64)
	+	Egr-1	(65)
PPAR γ	+	C/EBP α	(66)
	+	IRF-1	(67)
	+	Oct1	(68)
	-	AP-1	(69)
	-	E2F	(70)
	-	Egr-1	(71)
	+	CD38	(72)
	+	CD14	(73)
	+	p21	(74)
	-	p47Phox	(75)
PU.1	-	PPAR γ	(76)
	+	PU.1	(77)
	+	AP-1	(78)
	+	Egr-1	(32)
	+	CD11b	(79)
	+	p21	(80)
	+	p47Phox	(81)
C/EBP α	+	PPAR γ	(66)
	+	PU.1	(37)
	+	C/EBP α	(82)
	+	Gfi-1	(83)
	-	E2F	(84)
	+	CD14	(85)

894

	+	p21	(86)
IRF-1	+	CD38	(87)
	+	p21	(88)
	-	PU.1	(89)
	-	C/EBP α	(90)
	-	E2F	(90)
	-	Egr-1	(32)
	-	p21	(90)
Oct1	+	PU.1	(91)
AP-1	-	PPAR γ	(69)
	+	PU.1	(92)
	+	p21	(93)
E2F	+	E2F	(94)
Egr-1	+	PPAR γ	(95)
	-	Gfi-1	(96)
	+	CD14	(97)
AhR	+	AP-1	(98)
	+	IRF-1	(99)
	-	Oct4	(100)
	-	PU.1	

Table 2: Characteristic model parameters estimated from literature.

Symbol	Description	Value	Units	Source
R_1	RNA polymerase abundance	85,000	copies/cell	(101, 102)
R_2	Ribosome abundance	1×10^6	copies/cell	(103)
G_i	Characteristic gene abundance	2	copies/cell	this study
K_X	Saturation constant transcription	600	copies/cell	this study
K_T	Saturation constant translation	95,000	copies/cell	this study
$t_{1/2,m}$	characteristic mRNA half-life (transcription factor)	2-4	hr	(104)
$t_{1/2,p}$	characteristic protein half-life	10	hr	(105)
$\theta_{m,j}$	characteristic mRNA degradation constant	0.34	hr^{-1}	derived
$\theta_{p,j}$	characteristic protein degradation constant	0.07	hr^{-1}	derived
897				
t_d	HL-60 doubling time	19.5	hr	this study
μ	growth rate	0.035	hr^{-1}	derived
k_d	death rate	0.10μ	hr^{-1}	derived
e_T	elongation rate RNA polymerase	50-100	nt/s	(106–109)
e_X	elongation rate Ribosome	5	aa/s	(110)
$L_{T,o}$	characteristic gene length	15,000	nt	(111)
$L_{X,o}$	characteristic transcript length	5,000	nt	derived
k_T	characteristic transcription rate	1.44	hr^{-1}	derived
k_X	characteristic translation rate	3.60	hr^{-1}	derived
D	Diameter of an HL-60 cell	12.4	μm^3	(112)
f_C	cytoplasmic fraction	0.51	dimensionless	(112)

898 **Table 3:** Sequence lengths from NCBI RefSeq database was used in the signal integration and phenotype
 899 modules (113). The RNA sequence length used represents the total distance of transcription, and assume
 to be equal to the gene length.

Gene Name	Gene (bp)	RNA (bp)	Protein (AA)	Gene ID	Protein ID
AP-1	10323	10323	331	Gene ID: 3725	NP_002219
AhR	47530	47530	848	Gene ID: 196	NP_001621
CD11b	72925	72925	1153	Gene ID: 3684	NP_001139280
CD14	8974	8974	375	Gene ID: 929	NP_001035110
CD38	174978	74978	300	Gene ID: 952	NP_001766
C/EBP α	2630	2630	393	Gene ID: 1050	NP_001274353.1
E2F	17919	17919	437	Gene ID: 1869	NP_005216
900 Egr-1	10824	10824	543	Gene ID: 1958	NP_001955
Gfi-1	13833	13833	422	Gene ID: 2672	NP_005254
IRF-1	16165	16165	325	Gene ID: 3659	NP_002189
Oct1	206516	206516	741.33	Gene ID: 5451	NP_002688.3, NP_001185712.1, NP_001185715.1
Oct4	6356	6356	206.33	Gene ID: 5460	NP_001167002, NP_001167015, NP_001167016
P21	15651	15651	198	NG_009364.1	NP_001621
P47	3074	3074	390	GenBank: AF003533.1	NP_000256
PPAR γ	153507	153507	250	Gene ID: 5468	NP_001317544
PU.1	40782	40782	270.5	Gene ID: 6688	NP_001074016, NP_003111

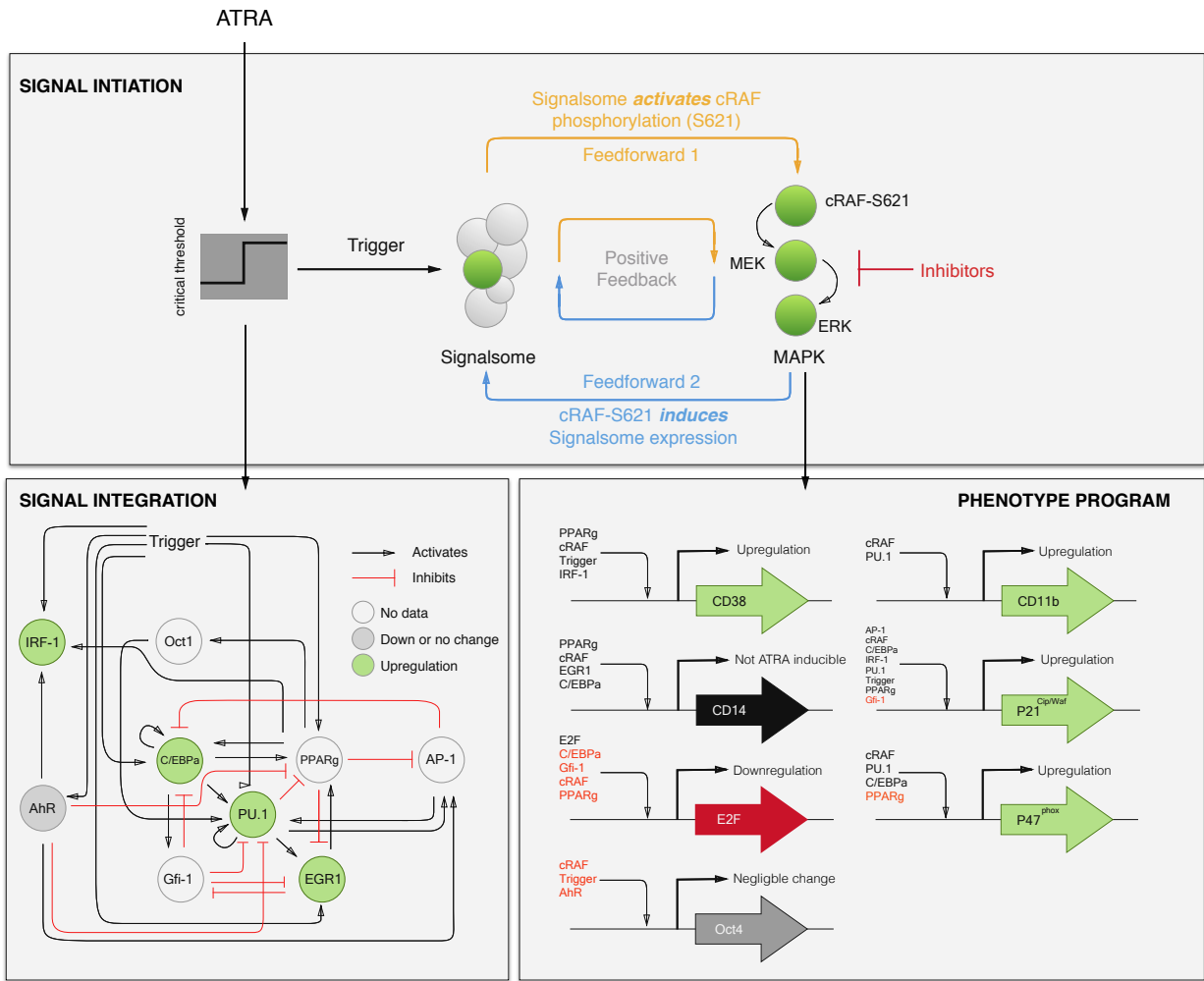


Fig. 1: Schematic of the effective ATRA differentiation circuit. Above a critical threshold, ATRA activates an upstream Trigger, which induces signalsome complex formation. Signalsome activates the mitogen-activated protein kinase (MAPK) cascade which in turn drives the differentiation program and signalsome formation. Both Trigger and activated cRaf-pS621 drive a phenotype gene expression program responsible for differentiation. Trigger activates the expression of a series of transcription factors which in combination with cRaf-pS621 result in phenotypic change.

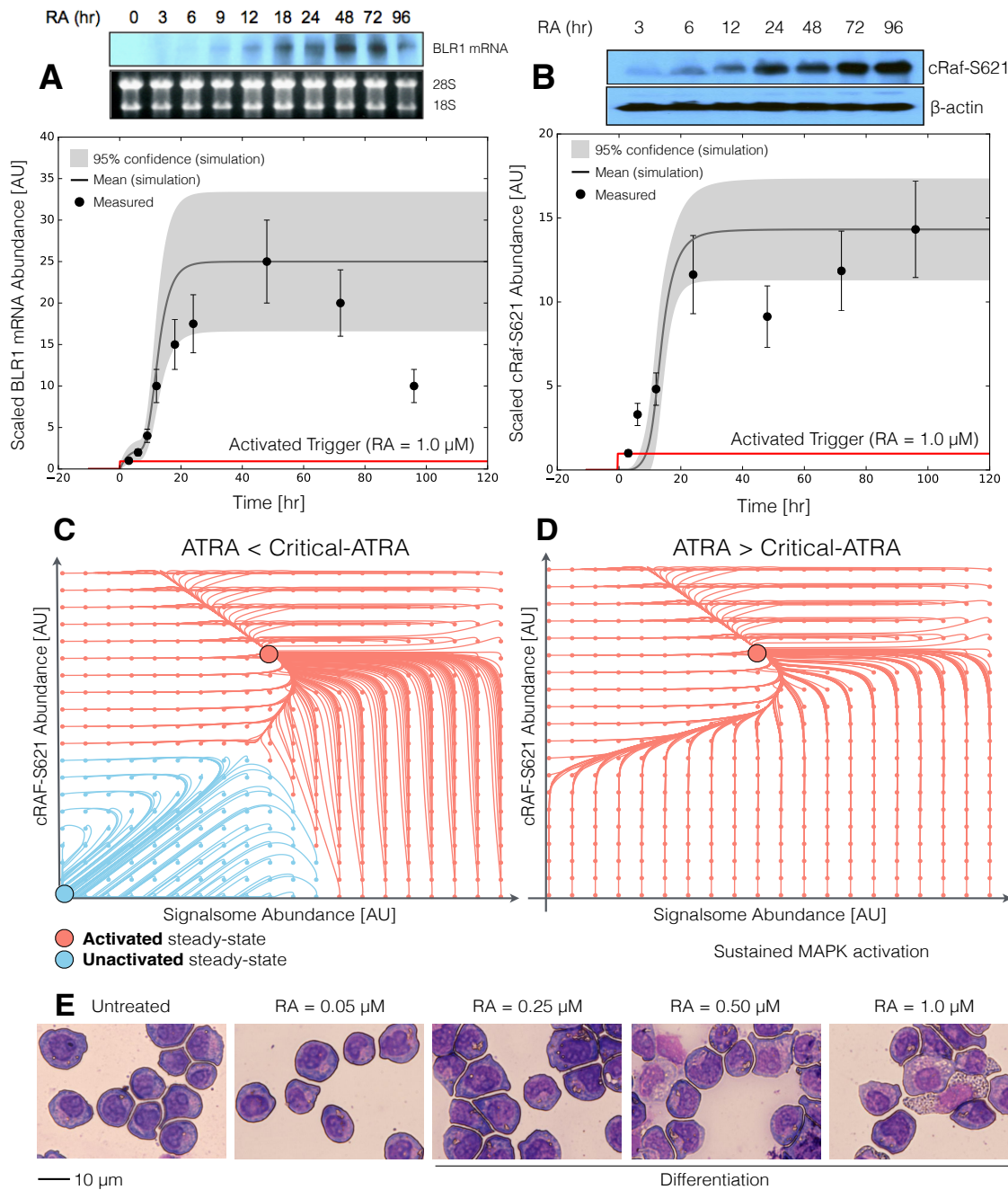


Fig. 2: Model analysis for ATRA-induced HL-60 differentiation. A: BLR1 mRNA versus time following exposure to 1 μ M ATRA at t = 0 hr. B: cRaf-pS621 versus time following exposure to 1 μ M ATRA at t = 0 hr. Points denote experimental measurements, solid lines denote the mean model performance. Shaded regions denote the 99% confidence interval calculated over the parameter ensemble. C: Signalsome and cRaf-pS621 nullclines for ATRA below the critical threshold. The model had two stable steady states and a single unstable state in this regime. D: Signalsome and cRaf-pS621 nullclines for ATRA above the critical threshold. In this regime the model had only a single stable steady state. E: Morphology of HL-60 as a function of ATRA concentration (t = 72 hr).

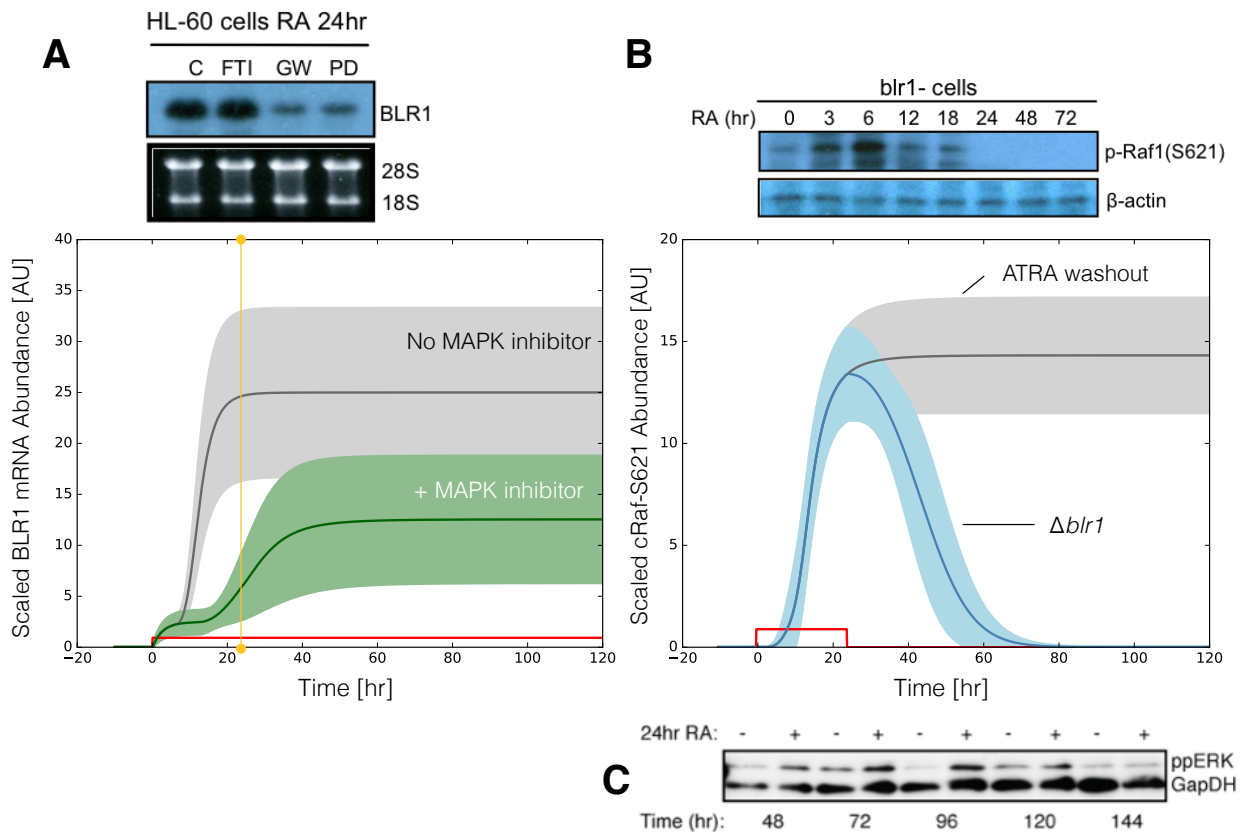


Fig. 3: Model simulation following exposure to $1\mu\text{M}$ ATRA. A: BLR1 mRNA versus time with and without MAPK inhibitor. B: cRaf-pS621 versus time following pulsed exposure to $1\mu\text{M}$ ATRA with and without BLR1. Solid lines denote the mean model performance, while shaded regions denote the 99% confidence interval calculated over the parameter ensemble. C: Western blot analysis of phosphorylated ERK1/2 in ATRA washout experiments. Experimental data in panels A and B were reproduced from Wang and Yen (20), data in panel C is reported in this study.

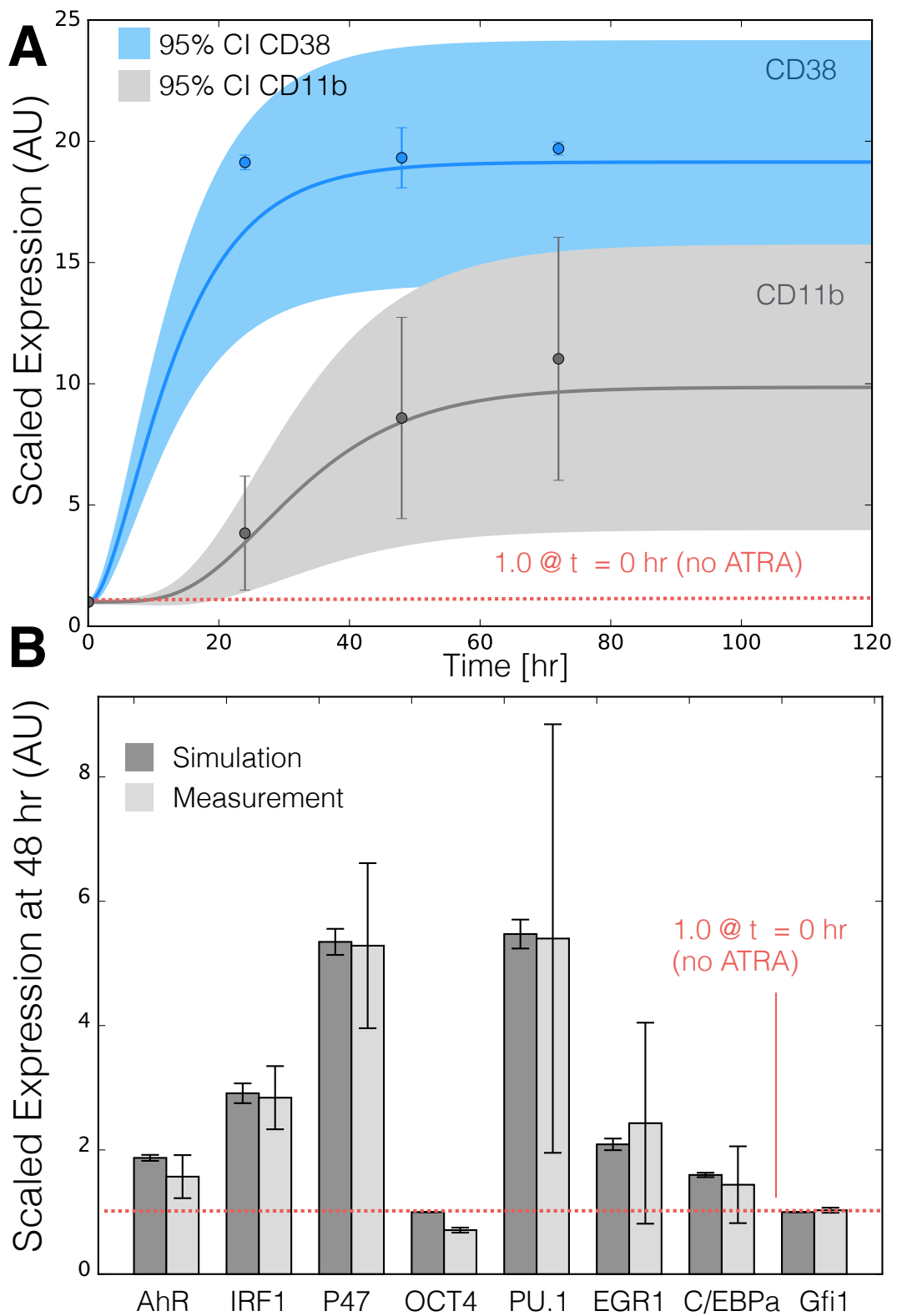


Fig. 4: Model simulation of the HL-60 gene expression program following exposure to $1\mu\text{M}$ ATRA at $t = 0$ hr. A: CD38 and CD11b expression versus time following ATRA exposure at time $t = 0$ hr. B: Gene expression at $t = 48$ hr following ATRA exposure. Experimental data in panels A and B were reproduced from Jensen et al. (25).

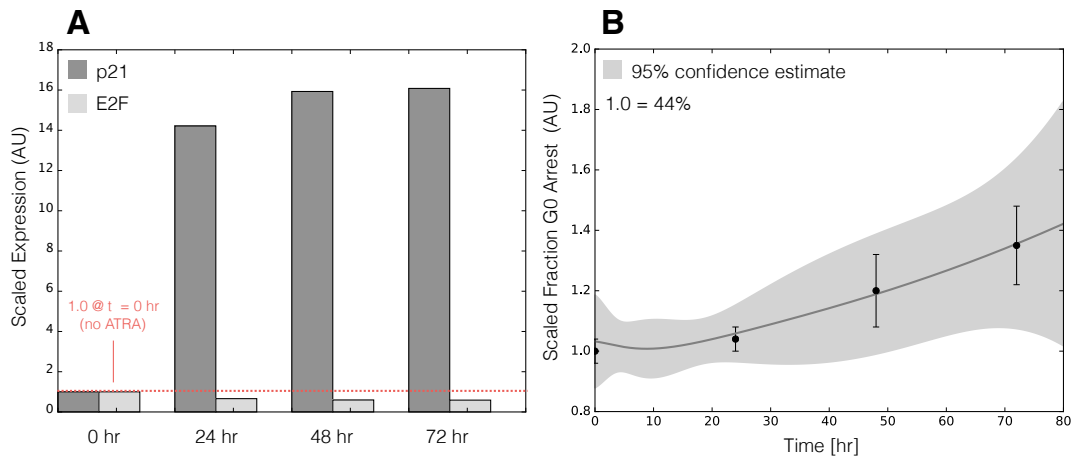


Fig. 5: Model simulation of HL-60 cell-cycle arrest following exposure to $1\mu\text{M}$ ATRA at $t = 0$ hr. A: Predicted p21 and E2F expression levels for the best parameter set following ATRA exposure at time $t = 0$ hr. B: Estimated fraction of HL-60 cells in G0 arrest following ATRA exposure at time $t = 0$ hr. The gray region denotes the 95% confidence estimate of the polynomial model. Experimental data in panel B was reproduced from Jensen et al. (25).

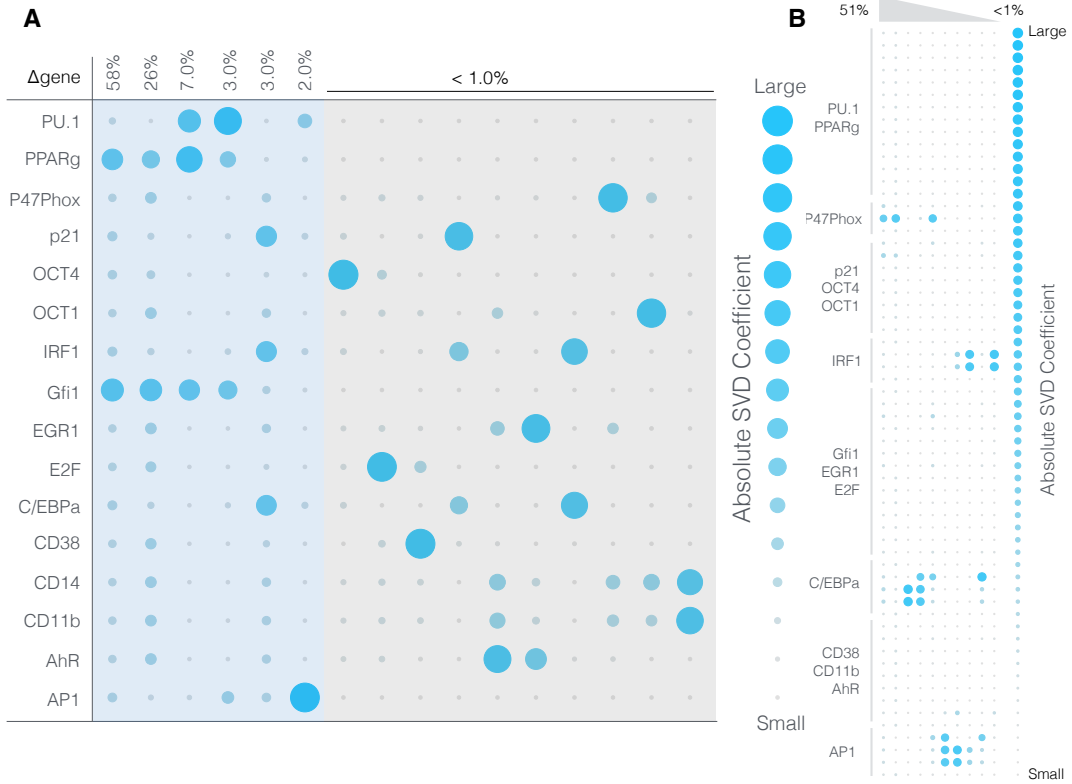


Fig. 6: Robustness of the HL-60 differentiation program following exposure to $1\mu\text{M}$ ATRA at $t = 0$ hr. A: Singular value decomposition of the system response (l^2 -norm between the perturbed and nominal state) following pairwise gene knockout simulations using the best fit parameter set. The percentage at the top of each column describes the fraction of the variance in the system state captured by the node combinations in the rows. B: Singular value decomposition of the system response (l^2 -norm between the perturbed and nominal state) following the pairwise removal of connections.

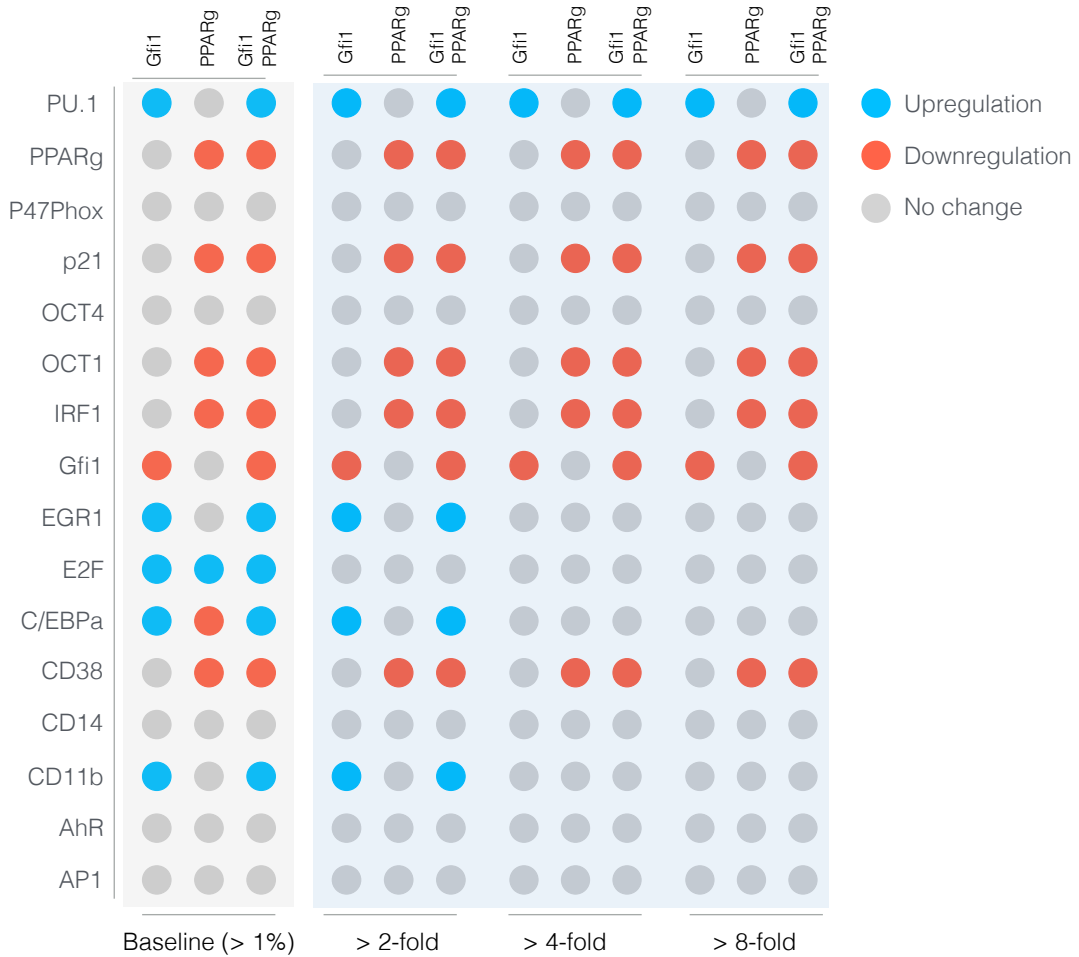


Fig. 7: Robustness of the HL-60 differentiation program following exposure to $1\mu\text{M}$ ATRA at $t = 0$ hr. Protein fold change at $t = 48$ hr (rows) in single and double knock-out mutants (columns) relative to wild-type HL-60 cells. The responses were grouped into >2,4 and 8 fold changes. The best fit parameter set was used to calculate the protein fold change.

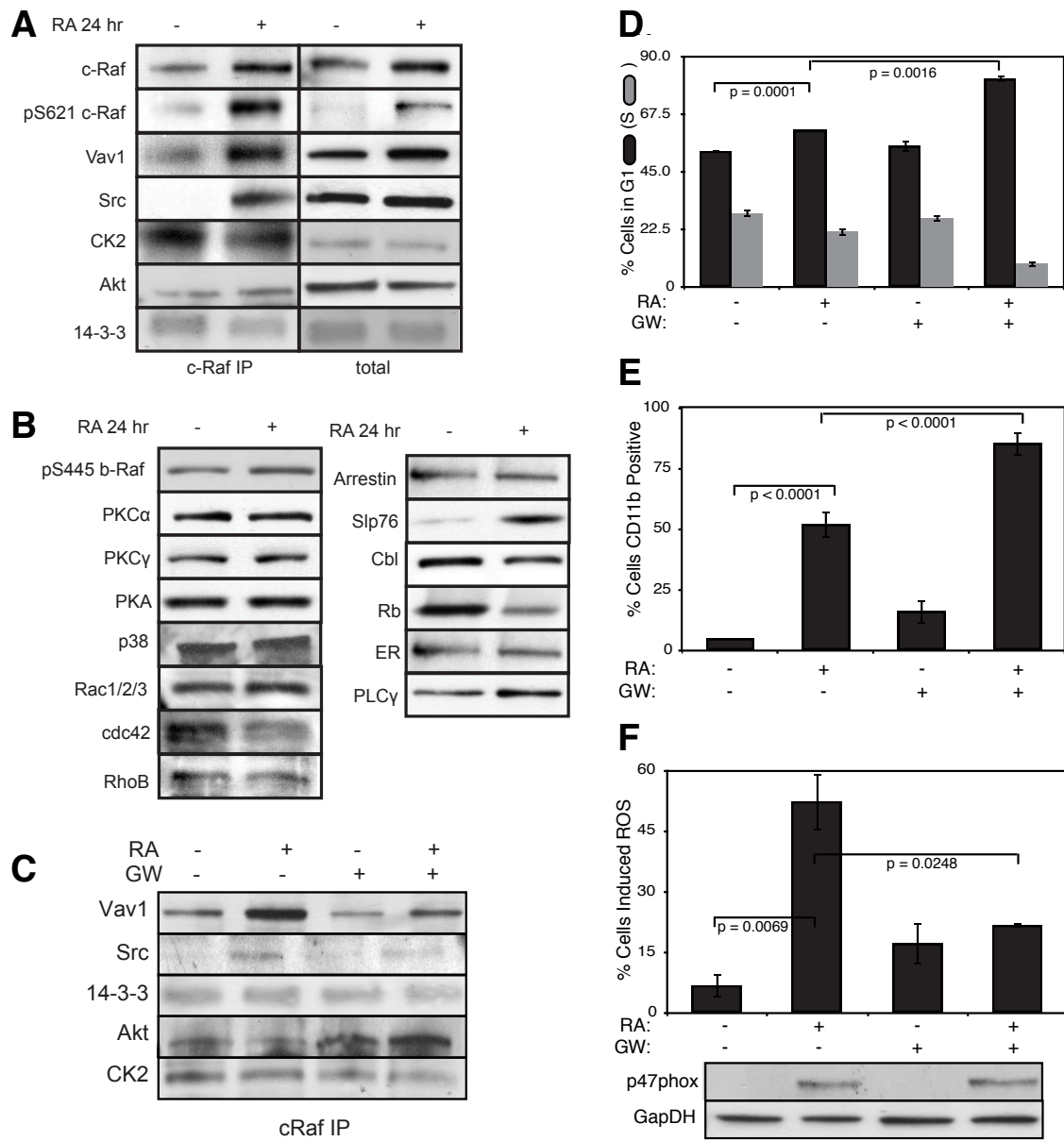


Fig. 8: Investigation of a panel of possible Raf interaction partners in the presence and absence of ATRA. A: Species identified to precipitate out with Raf: first column shows Western blot analysis on total Raf immunoprecipitation with and without 24 hr ATRA treatment and the second on total lysate. B: The expression of species considered that did not precipitate out with Raf at levels detectable by Western blot analysis on total lysate. C: Effect of the Raf inhibitor GW5074 on Raf interactions as determined by Western blot analysis of total Raf immunoprecipitation. The Authors note the signal associated with Src was found to be weak. D: Cell Cycle distribution as determined by flow cytometry indicated arrest induced by ATRA, which was increased by the addition of GW5074. E: Expression of the cell surface marker CD11b as determined by flow cytometry indicated increased expression induced by ATRA, which was enhanced by the addition of GW5074. F: Inducible reactive oxygen species (ROS) as determined by DCF flow cytometry. The functional differentiation response of ATRA treated cells was mitigated by GW5074.